# Prediction and Mitigation of the Mode Transition in a Magnetically Shielded Hall Thruster at High-Specific Impulse and Low Power

**IEPC-2022-372**

*Presented at the 37th International Electric Propulsion Conference*
*Massachusetts Institute of Technology, Cambridge, MA, USA*
*June 19-23, 2022*

Benjamin A. Jorns,[1] Matthew Byrne,[2] Parker Roberts,[3] Leanne Su,[4] Ethan Dale [5]
*University of Michigan, Ann Arbor, MI, 48109*

Richard R. Hofer [6]
*Jet Propulsion Laboratory, California Institute of Technology, Pasadena, CA, 91109*

**The mode transitions of discharge current oscillations in a 9-kW class magnetically shielded Hall thruster are experimentally and theoretically investigated. It has been found that when a shielded thruster designed for operation at a fixed power level and high specific impulse (> 2000 s) is operated at less than 60% of the nominal power, the discharge current oscillations exhibit a transition to a highly oscillatory state. This is characterized by peak-to-peak amplitudes greater than 100% of the mean discharge current and frequencies ranging from 10-20 kHz. These properties are consistent with the canonical Hall thruster breathing mode. A quasi-0D, two-equation model for this breathing mode oscillation in shielded thrusters is derived based on simplifying assumptions informed by experimental measurements of plasma properties in the channel. The stability margin of the thruster is then experimentally characterized for discharge voltages from 300-600 V and discharge currents from 5-15 A. The model is calibrated and validated against these results and shown to predict quantitative trends in the stability margin and qualitative trends in the frequency of oscillation. An analytical stability criterion that depends on discharge voltage and current is derived based on this model, which is employed to inform mitigation strategies for the mode transition. These strategies, which include changing the anode temperature and magnetic field strength, are experimentally assessed and shown to shift the transition point by 1-2 A ($\sim 10-15\%$) in discharge current at a discharge voltage of 600 V. These results and the model are discussed in the context of the simplifying assumptions, the extensibility of the model to other operating conditions, and the implications of the result for ground test efforts and thruster design.**

## I. Introduction

The extended lifetime of magnetically-shielded (MS) Hall thrusters [1–3] combined with their high specific impulse (> 2000 s) and moderate thrust density is an enabling feature for a wide range of interplanetary missions. To meet the requirements of deep space maneuvers, however, shielded thrusters must be capable of maintaining high performance (efficiency and specific impulse) as the input power decreases. This stems from the fact that as a spacecraft spirals from the sun, the solar power available to the propulsion system falls. In practice, however, if MS thrusters are throttled below 60% the nominal design power at high specific impulse (> 2000 s), previous studies have shown they can undergo a

[1]Associate Professor, Aerospace Engineering
[2]Doctoral Candidate, Aerospace Engineering
[3]Doctoral Candidate, Aerospace Engineering
[4]Doctoral Candidate, Aerospace Engineering
[5]Former Doctoral Candidate, Aerospace Engineering, Currently Technical Staff at Aerospace Corporation
[6]Principal Engineer and Supervisor, Electric Propulsion Group

mode transition characterized by large amplitude (> 100% background) and high frequency (~ 10-50 kHz) oscillations in the discharge current These oscillations can cause life-limiting damage to the thruster and pose a major risk for deep space applications. Faced with this potential limitation and in light of the advantages of low-power, high-specific impulse MS thrusters for deep space applications, there is a pressing need to understand this mode transition and mitigate it.

The frequency and amplitude of the mode transition exhibited at low power suggest that it may be a form of the classical breathing mode oscillation [4, 5]. This instability appears in nearly all Hall effect thrusters and has been the subject of extensive numerical[6–22] and experimental study [23–35, 35–38]. The conventional description of this oscillation [6] is that it is related to ionization in the Hall thruster channel. The neutral and plasma density in this region are described by a predator-prey cycle that results in periodic fluctuations in the discharge current. With that said, while there is largely consensus about the physical interpretation of the wave as ionization related, the stability criteria for the onset of the breathing mode remains an open question. Several theories have been proposed to date including that the destabilizing element is related to energy balance to the walls [7, 16], ion flux to the anode [21], time delay between ionization in the region near the anode versus in the acceleration zone [8, 11, 13, 38, 39] and nonlinear coupling between the electric field and density and current [9, 22]. Yet, while many of these previous simulations and theoretical analyses were able to re-create the breathing mode for some operating conditions, there is not consensus about what the dynamics of this oscillation. This lack of understanding poses a particular challenge for trying predict the oscillation in new operating regimes for the Hall thruster like the high specific impulse, low power condition of interest in this work.

The goal of this study is to investigate theoretically and experimentally the breathing mode transitions in a magnetically shielded Hall thruster. To this end, we begin in Sec. II by formulating a simple quasi-0D, two-equation model for this instability that is informed by direct experimental measurements in a Hall thruster channel. The resulting model is identical to the simplified two equation model proposed by Barral and Peradzynski[11]. In Sec. III, we describe our experimental configuration for characterizing the oscillations in a shielded thruster. Then, in Sec. IV, we experimentally assess the stability margin in a 9-kW shielded Hall thruster over a range of discharge voltages and discharge currents. We use these results to calibrate and validate our quasi-0D model. In Sec. VI, we leverage this model to explore experimentally possible mitigation techniques for the oscillation at high specific impulse (discharge voltage) conditions. Finally, in Sec. VI, we discuss the implications and limitations of our analysis and possible extensions to further mitigate the mode transition at high specific impulse and low power operation.

## II. Quasi-0D model for the breathing mode oscillation

We present in the following an empirically-motivated quasi-0D model for the breathing mode dynamics in the channel of a magnetically shielded Hall thruster. To this end, we begin by reviewing experimental measurements from our previous work [38] for time-resolved plasma properties in the channel of a magnetically-shielded Hall thruster. We then use these experimental measurements to propose and evaluate the validity of fluid-based governing equations for the fluctuations. This then motivates a reduced fidelity, two-equation model we employ for evaluating thruster stability.

### A. Thruster geometry

Fig. 1 shows a canonical geometry of a Hall thruster cross-section. The device consists of an axial electric field applied across a confining radial magnetic field in a discharge channel of width, $w$, and average radius, $r$. Neutral density propagates from an upstream manifold where it is then impact ionized by electrons in the plasma. The region where this occurs is denoted as the "ionization zone." The resulting ions are then accelerated out of the geometry by the applied electric field. This region is denoted as the "acceleration zone." In the following discussion, we invoke experimental measurements to more formally define the extent of these two regions.

### B. Review of previous 1D, time-resolved experimental measurements in channel

In our previous work, we employed a combination of laser induced fluorescence and a far-field current density probe to characterize the time resolved plasma and neutral properties along the channel centerline of a Hall thruster (Fig. 1) on the timescale of the breathing mode oscillation. The device in this study (Sec. III was the H9, a magnetically shielded thruster, that we operated at 3 kW and 300 V discharge voltage. The details of the experimental technique can be found in Ref. [38]. In brief, the method is based on solving the ion momentum and continuity equations by employing experimentally-measured moments of the ion velocity distribution and ion flux density. These solutions then are coupled with the neutral continuity equation and an electron Ohm's law to yield a set of spatially and time-resolved measurement of plasma and neutral density, electron temperature, ion and neutral velocity, and electrical field along

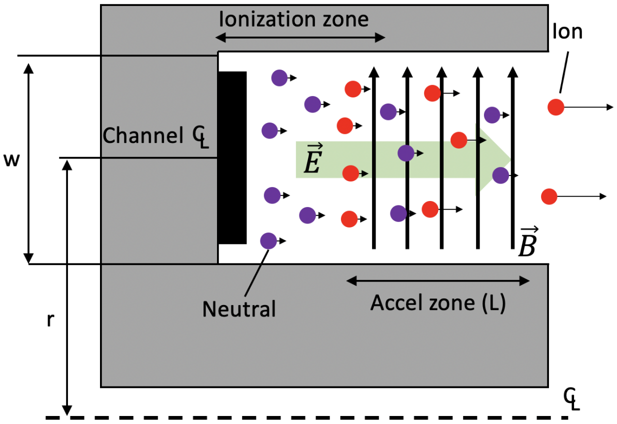


**Fig. 1 Canonical geometry of Hall thruster cross-section illustrating electric and magnetic fields, ionization zone, and acceleration zone.**

channel centerline. Fig. 2 shows examples of the results of this method where we depict spatio-temporal plots of discharge current, ion velocity, and neutral density. Here, we have shown the property as a function of axial distance along the channel and as a function of phase of the discharge current oscillation. Using phase dependence is a result of the analysis method, which is based on a phase-sensitive transfer function referenced with respect to the discharge current. The frequency of the oscillation was $\sim 16$ kHz.

The plasma properties shown in Fig. 2 all oscillate on the timescale of the breathing mode oscillation. The discharge current is uniform in the axial direction. This is a result of current continuity in the thruster, which is ensured by the fact that the walls are non-conducting. Physically, this figure emphasizes the fact that current oscillations are non-local in the plasma. This is a point we return to in the following sections. The plasma ion velocity shown in Fig. 2 also oscillates on the timescale of the discharge current, with a waveform characterized by a periodic shift in the location of the zone. With that said, we note that the upstream and downstream velocities remain approximately constant over the period of oscillation, starting nearing the ion sound speed and accelerating to ~ 20 km/s. The oscillations in turn occur in a spatially confined region. We denote the boundaries of this region with the dashed lines and refer to it as the "acceleration zone" for the remainder of this work.

Fig. 1c shows the time resolved fluctuations in neutral density. As shown here and demonstrated in Ref. [38], these oscillations are characterized by the propagation of perturbations downstream at approximately the neutral velocity. Notably, these fluctuations, which are $> 50\%$ of the mean value, have a high amplitude in the region upstream of where we have defined the acceleration zone. As we suggested in Ref. [38], this may indicate these modes are causally originating upstream of this region. As a significant degree of ionization evidently is occurring here, we denote this region, consistent with Fig. 1, as the ionization region. The fact that the ionization and acceleration zones appear to be spatially distinct yet but fluctuating is a key element we invoke in the following discussion.

### C. Experimental measurements of 0D plasma properties in acceleration zone

In this section, we convert the 1D time resoled measurements from Ref. [38] into 0D time-resolved fluctuations in the channel. We then attempt to find governing relations informed by fluid theory for the timing and phasing of these relations. To this end, we first spatially averaged the measured plasma properties over the acceleration zone shown in Fig. 2. Fig. 3 shows as a function of phase the resulting spatially-averaged measurements of plasma density, $\langle n_i \rangle$, neutral density, $\langle n_n \rangle$, axial ion velocity,$\langle u_i \rangle$, electron temperature, $\langle T_e \rangle$, axial electric field, $\langle E_z \rangle$, and discharge current, $I$. Here $\langle .. \rangle$ denotes spatial average for the indicated quantity. The neutral velocity is not depicted, as this was approximately constant over the period of oscillation.

This result shows that all the plasma quantities, except the neutral velocity, oscillate on the timescale of the breathing mode oscillation. We in turn can comment qualitatively on the exhibited trends. For example, the average electric field, ion velocity, and electron temperature all are approximately in phase. The correlation between electric field and ion velocity is intuitive as the electric field is the dominant driving force for ion acceleration. Similarly, the primary source of electron thermal energy in the channel is Ohmic heating driven by the electric field. The strong in-phase correlation

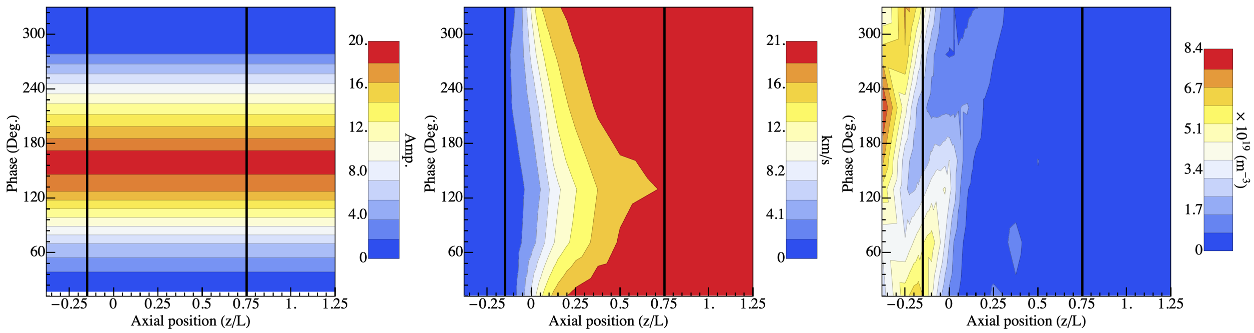


(a) (b) (c)

**Fig. 2 Contour maps of plasma properties along channel centerline as a function of phase of the discharge current oscillation for the H9 thruster at 300 V and 10 A. Depicted properties include a) discharge current, b) ion velocity, and c) neutral density. The spatial resolution is approximately 2 mm while the phase resolution is $50°$. Spatial coordinates have been normalized to channel length and referenced with respect to the exit plane. The vertical lines denote our specification for the boundaries of the acceleration zone. Data adapted from Ref. [38]**

between these two spatially averaged properties underscores this relationship. In contrast, the electric field and discharge current are anti-correlated in time. This observation, which is consistent with some previous numerical simulations (c.f. [7, 8]), suggests that the electron resistivity dynamically changes in the thruster on the timescale of the breathing mode oscillation. We otherwise would expect from a generalized Ohm's law that the current and electric field should scale. To this point, it previously has been documented experimentally that the electron mobility is a dynamic function of the breathing mode oscillation [35]

As another notable trend, we see the neutral density fluctuations lead the plasma density fluctuations by approximately 45 degrees. This out of phase relationship is characteristic of the typical "predator-prey" interpretation of the breathing mode. As neutral density is depleted by ionization, the plasma density increases [6]. With too low neutral density, however, ionization decreases, and the neutral density can refill the volume. Eventually, with sufficient replenishment, ionization resumes, and the cycle repeats.

Finally, we note that the plasma density and discharge current are highly correlated and in-phase while the ion velocity is anti-correlated with both current and plasma density. We will expand on the significance relationship in the next section as it suggests that the dominant driver for the current is the change in density of the species rather than speed. This allows us to motivate a simplified description for the dynamics.

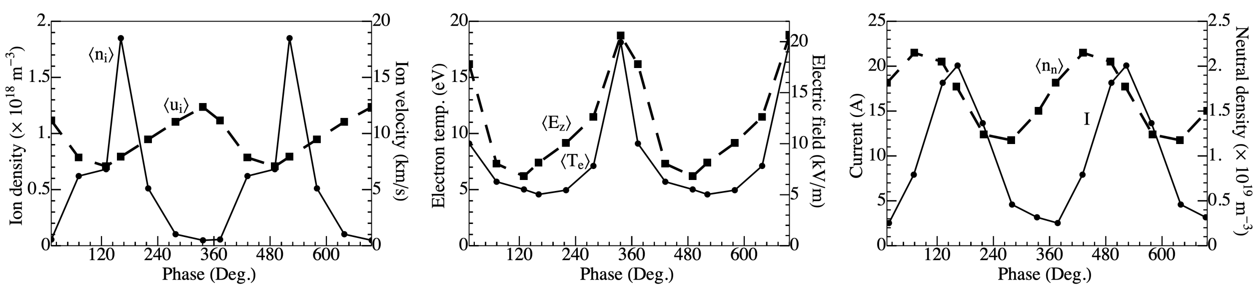


(a) (b) (c)

**Fig. 3 Spatially-averaged centerline measurements of a) plasma density and ion velocity, b) electric field and electron temperature, and c) current and neutral density in the acceleration zone as a function of phase of the discharge current oscillation.**

### D. Governing equations for 0D model properties

Now that we have established experimentally the time-averaged plasma properties in the channel, we use these results to inspire a dynamical model for their evolution. Indeed, while a full description of the plasma oscillation could require a multi-dimensional fluid or kinetic model, we can employ the trends shown in the previous section to make assumptions that allow for a simpler and more easily evaluated dynamical description. Our overarching goal in this case is to find a set of relations for the neutral density and discharge current. These parameters are both critically linked to the oscillation and have previously formed the basis for models for this mode [11].

Before proceeding with this approach, we remark that these simplifications are ultimately at the expense of fidelity, and in some cases, are not understood from first principles. The anti-correlation between current and electric field alluded to in the preceding section is a notable example. With that said, absent a first-principles understanding of relationships like these, at least for the operating condition we consider here, we can still use the observation of the empirical phase relation to make simplifying assumptions.

#### *1. Discharge current scaling with plasma density*

We first consider a governing equation for the discharge current. This is the property most easily assessed during thruster operation (without the need for internal probes) and is often used as the metric for identifying the onset of the breathing mode. The current can be represented in terms of channel-averaged properties as

$$I = qA\langle n_i\rangle\left(\langle u_i\rangle - \langle u_e\rangle\right), \tag{1}$$

where $I$ denotes discharge current, $q$ is fundamental charge, $A$ is the cross-sectional area of the channel, $\langle n_i\rangle$ is the spatially averaged ion density along centerline, $\langle u_i\rangle$ is the average speed in the axial direction and $\langle u_e\rangle$ is the average electron velocity in the axial direction. We note that we have assumed in this representation that the plasma is dominated by singly charged ions.

Based on the trends from Fig. 3 the density correlations are highly correlated with the discharge current while anti-correlated with the ion velocity. Moreover, the relative fluctuations in average velocity are only 20% of the mean while the density fluctuations approach 100%. This leads us to make the ansatz that the evolution of the current is governed primarily by the plasma density. We thus can approximate

$$\frac{I}{I_0} \approx \frac{\langle n_i\rangle}{n_{i(0)}}, \tag{2}$$

where $I_0$ and $n_{i(0)}$ denote the time-averaged current and ion density in the channel. We show the left and right sides of this relation in Fig. 4a, where we see both exhibit similar trends in phase and amplitude. The shape of the density fluctuations is ultimately more staggered, though we remark this may in part stem from the relative coarseness of the data in time. Indeed, to this point, when we perform a running average on the datasets with a width of three data points, we find even more marked agreement. This is shown in Fig. 4b. We note here that in making this approximation, we have not elucidated the reason why the ion velocity is anti-correlated and smaller than the fluctuations in ion density (thus enabling this simplification). This would require a higher fidelity analysis of the underlying physics. Rather, we simply invoke the experimental result to proceed with our simplified analysis.

#### *2. Governing equation for discharge current*

Given Eq 2, we next motivate a governing equation for the time evolution of the discharge current. To this end, we take the time derivate of this relation:

$$\frac{dI}{dt} \approx \frac{I_0}{n_{i(0)}}\frac{d\langle n_i\rangle}{dt}. \tag{3}$$

We in turn can employ the continuity equation for ions (neglecting recombination) volumetrically averaged over the acceleration zone (Fig. 1) to write

$$\gamma\frac{d\langle n_i\rangle}{dt} = -\beta\left(\frac{\langle u_i\rangle}{L} + 2\frac{\langle c_s\rangle}{w}\right)\langle n_i\rangle + \alpha\langle n_i\rangle\langle n_n\rangle\langle\zeta_{iz}(T_e)\rangle, \tag{4}$$

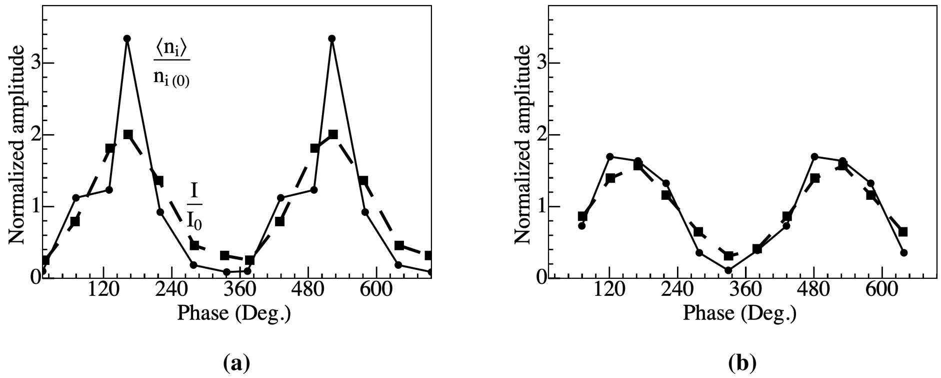


**Fig. 4 Comparison of the normalized discharge current oscillations and density fluctuations as a function of phase from a) raw data and b) with a three point moving average.**

where $c_s = \sqrt{q\langle T_e\rangle/m_i}$ denotes the average ion sound speed with ion mass, $m_i$, and $\langle\zeta_{iz}\rangle$ denotes the ionization rate coefficient. This is a function of the average electron temperature: [40]:

$$\zeta_{iz}(T_e) = \left(-10^{-24}T_e^2 + 6.386\times 10^{-20}e^{-\frac{12.13}{T_e}}\right)\sqrt{\frac{8qT_e}{\pi m_e}}, \tag{5}$$

where $m_e$ is the electron mass and $T_e$ is units of electron temperature. We also have introduced constants, $\alpha$, $\beta$, and $\gamma$ in the equation that are order unity. These are geometric factors that correct for the fact that the data is spatially-averaged along the channel centerline while the averages in Eq. 4 are volumetric, e.g. $\int_V n_i dV = A\gamma\int_0^L n_i dz = AL\gamma\langle n_i\rangle$ where $z$ denotes the location along channel centerline and $V$ is the channel volume. Similarly, the constants $\beta$ and $\alpha$ are inserted in recognition that the spatial average of the product quantities does not necessarily equal the product of the spatial averages of each term.

Invoking Eq. 2 and combining with Eq. 3, we find

$$\gamma\frac{dI}{dt} = I\left[\alpha\langle n_n\rangle\langle\zeta_{iz}(T_e)\rangle - \beta\left(\frac{\langle u_i\rangle}{L} + 2\frac{\langle c_s\rangle}{w}\right)\right] \tag{6}$$

Physically, the first term on the right of this relation represents the creation of charge per unit due to ionization in the acceleration zone. This has the net effect of increasing the current. The second term represents the loss of current due to flux of the plasma out of the channel to the exit (first term in the quantity) and walls (second term). In formulating the wall loss term, we have assumed the ions flux to the walls through a pre-sheath that accelerates them to the ion sound speed. This is consistent with typical boundary condition models employed in Hall thruters [40].

To further simplify Eq. 6, we again examine the trends in Fig. 3 where we see that with the exception of the neutral density, all the parameters in the quantity in Eq. 6 are nearly 180 degrees of phase with the discharge current oscillations. The product of the oscillating components of these quantities with the discharge current (as indicated on the right side of Eq. 6) thus will approximately cancel, yielding no net change in discharge current with time. The only relevant fluctuating quantity based on the experimental data thus to include in Eq. 6 is the time-dependence of neutral density:

$$\gamma\frac{dI}{dt} = I\left[\alpha\langle n_n\rangle\zeta_{iz}(T_{e(0)}) - \beta\left(\frac{u_{i(0)}}{L} + 2\frac{c_{s(0)}}{w}\right)\right], \tag{7}$$

where we have introduced time-averaged quantities denoted with the subscript, "0". We remark again that we have employed the empirical trends to justify this simplification, though the physical basis underlying the anti-correlation between the plasma properties and current is not investigated further here.

With this in mind, we can simplify Eq. 7 to

$$\frac{dI}{dt} = \bar{\alpha}I\zeta_{iz}(T_{e(0)})\left[\langle n_n\rangle - n_{n(0)}\right], \tag{8}$$

where we have defined the time-averaged background neutral density, $n_{n(0)} = (\alpha\gamma\zeta_{iz}(T_{e(0)}))^{-1}\beta\left(\frac{u_{i(0)}}{L} + 2\frac{c_{s(0)}}{w}\right)$ and collapsed the constants into a modified, $\bar{\alpha} = \alpha/\gamma$. This final expression is the same relation found by Barral and Peradzynski [11] in proposing a simplified quasi-0D model for the discharge current fluctuations. In this previous work, the authors arrived at this form by linearizing a non-localized model for the 1D plasma response to density and current fluctuations. To find the 0D form, the other plasma properties were assumed to be approximately constant spatially and in time in the acceleration zone. While this is not explicitly required in our assumptions here (rather we have invoked arguments about the phasing of fluctuations), the functional result is the same.

To evaluate the validity of Eq. 8 in describing our plasma dynamics, we show in Fig. 5 a comparison of the experimental measurements of the time derivative of the discharge current and the right side of Eq. 8. We have used the value $\bar{\alpha} = 0.5$ to best fit the data. The trends in Fig. 5 show that the two relations are nearly co-aligned. This suggests that this simplified relation represents the dynamics in the acceleration zone for the discharge current oscillations.

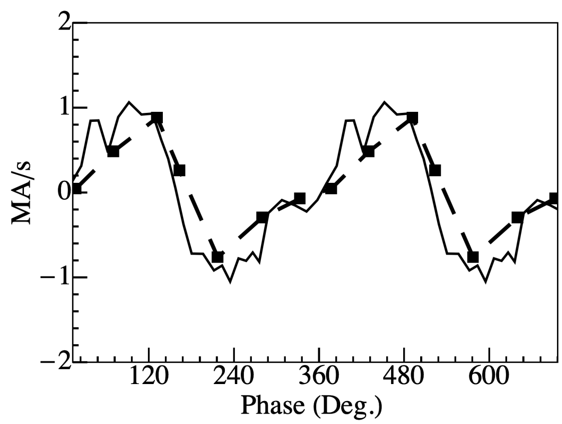


**Fig. 5 Comparison of the derivative of discharge current (solid) with the right side of Eq. 8. The best fit parameter $\bar{\alpha} = 0.5$ is employed.**

*3. Governing equation for neutral density*

As a next step, we consider the dynamics of the neutral oscillations. This also can be represented with a 0D, continuity equation that results from performing a volumetric average over the channel:

$$\frac{d\langle n_n\rangle}{dt} = \delta_1\frac{\Gamma_{in}}{AL} - \delta_2\langle n_n\rangle\langle n_i\rangle\langle\zeta_{iz}(T_e)\rangle, \tag{9}$$

where $\Gamma_{in}$ represents the flux of neutrals from the region upstream of the acceleration zone (left of Fig. 1) and the second term on the right side represents the loss of neutral density due to ionization. In deriving this result, we have assumed that the relative loss of neutrals fluxing out of the acceleration zone compared to the inlet flux in is negligible–i.e. there is a high degree of mass utilization. As with Eq. 4, we also have introduced in this result geometric factors, $\delta_1$ and $\delta_2$, of order unity that account for the disparity between the channel and volume averaged values of the indicated quantities. To relate this result to our other parameter of interest, discharge current, we eliminate the ion density from Eq. 9 by invoking Eq. 2 to find

$$\frac{d\langle n_n\rangle}{dt} = \delta_1\frac{\Gamma_{in}}{AL} - \delta_2 n_{i(0)}\langle n_n\rangle\frac{I}{I_0}\zeta_{iz}(T_{e(0)}), \tag{10}$$

where in parity with Eq. 8, we have eliminated the time dependence of the ionization rate.

One of the major challenges in previous treatments of the form of Eq. 10 has been identifying the form of the neutral influx. It has been proposed, for example, that this term should be constant, scaling with the inlet flow rate, $\Gamma_{in} = \dot{m}/m_i$ [10, 16]. This reflects the assumption that ionization occurs predominantly in the acceleration zone. Subject to this assumption, we show in Fig. 6a the left and right sides of Eq 10. Here we have employed the length, $L$, from the region defined in Fig. 1 and adjusted the scaling parameters, $\delta_1$ and $\delta_2$ to achieve the best qualitative match between the two trends. We see from this result that while the amplitude is comparable, there is evidently a phase delay of approximately 45° between the trends. This suggests that this governing equation does not accurately capture the timing of the oscillation.

To verify that this disagreement is not an artifact of the simplifying assumptions we have made, we also show the full relation from Eq. 9 allowing for time varying rate coefficient and plasma density. We still see from this result that the phase delay and shape persist. This underscores the fact that this governing equation with a fixed mass influx does not capture the 0D dynamics. This conclusion is not unexpected, however, given that previous authors have shown that assuming a constant influx can lead to unphysical damping of the oscillation [41].

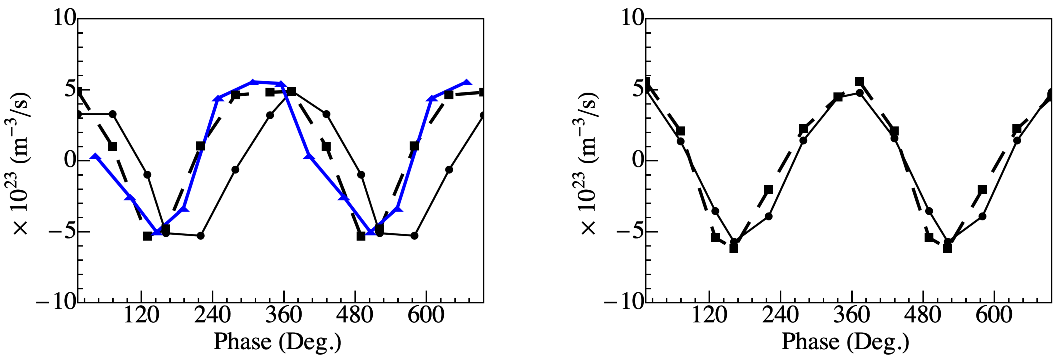


**(a)** **(b)**

**Fig. 6 a) Comparison of the derivative of neutral density (solid) with the right sides of Eq. 9 (blue) and Eq. 10 (dashed) assuming a constant influx of neutral flow. The best fit coefficients are $(\delta_1, \delta_2) = (4.2, 2.2)$ and $(2.7, 3.1)$ for the Eq. 9 (blue) and Eq. 10 (dashed) solutions respectively. b) Comparison of the derivative of neutral density (solid) with the right side of Eq. 10 (dashed) assuming a time-dependent influx of neutral flow. The best fit coefficients are $(\delta_1, \delta_2) = (2.7, 3.1)$.**

.

With this in mind, we can add fidelity to the simulation by allowing the flux term to the ionization zone to be time dependent, $\Gamma(t)$. Indeed, this is the critical assumption by Barral [11, 13], which led to the ability to capture oscillations self-consistently from their simple dynamical model. Following this approach, we remark that one reason the inlet neutral density to the acceleration zone can oscillate is due to ionization that occurs upstream of the acceleration zone. Indeed, even though the electron temperatures are relatively low in this upstream region near the anode, given the high neutral densities, ionization rates are actually the highest in the thruster in this region. To this point, we already have marked from Fig. 2c that substantial (> 50% of mean) neutral density fluctuations occur upstream of the region we have defined as the acceleration zone. These variations in neutral density then propagate downstream at approximately the neutral drift speed [38]. This effectively translates to a time-dependent variation of the inlet flux to the acceleration zone.

With this in mind, we show in Fig. 6b the case when we replace the flux term with $\Gamma = \langle n_{n(in)} \rangle u_n A$. Here $u_n \approx 200$ m/s is the neutral velocity, and we denote $\langle n_{n(in)} \rangle$ as the average neutral density over the six spatial locations immediately adjacent to the line we denoted as the upstream boundary of the acceleration zone in Fig. 2). As Fig. 6b illustrates, the comparison of the left and right sides of Eq. 10 shows marked improvement in the agreement of amplitude and phase agreement when we account for the time-dependent inlet flux.

The physical interpretation of this result is that the oscillations in the neutral influx (first term on right side of Eq. 10) introduce a phase delay with respect to the oscillations resulting from ionization in the acceleration zone (second term on right side of Eq. 10). This phase delay stems from the fact that the neutral density in the ionization zone oscillates on the same timescale as the ionization rates in the acceleration zone, but the resulting perturbations propagate slowly from the upstream region (at neutral speed) to the acceleration zone. As Barral discussed [11] and we expand on in Sec. VI, the relative timing of the arrival of the inlet neutral density to the acceleration zone can enable positive feedback with the oscillations already occurring in region. This in turn promotes the growth of the instability.

*4. Governing equation for inlet flux*

While the insight from the preceding section may explain the destabilizing mechanism for the instability, in practice, describing the neutral density in the ionization zone (Fig. 1) requires that we introduce an additional relation. Unfortunately, unlike in our preceding analysis, we do not have detailed experimental measurements over the extent of this region to inform a derivation of simplified governing equation. Absent this data, we instead adapt the model proposed by Barral et al [11] for the neutral dynamics in the upstream region. This is predicated on the following assumptions:

- The electron temperature is only weakly varying spatially in the ionization region. This is consistent with the fact that the ionization zone is upstream of the region where most of the Ohmic heating in the thruster occurs, i.e. where the electric field is highest.
- As with Eq. 3, there is linear scaling between discharge current and plasma density in this region.
- The inlet mass flow to the ionization zone (coincident approximately with the anode) is given by $\dot{m}$
- Recombination at the anode is neglected.
- The neutral speed, $u_n$ is constant in this region.

Subject to these assumptions, the 1D neutral continuity equation in the ionization zone yields

$$n_{n(in)} = \frac{\dot{m}}{m_i}\frac{1}{u_n A}\exp\left[-\frac{1}{I_0}n_{i(0)}^{ion}\zeta_{iz}(T_{e(0)}^{ion})\int_{t-\tau_n}^{t} Idt\right], \tag{11}$$

where $\tau_n$ is the transit time of the neutrals from the anode to the acceleration zone, $n_{i(0)}^{ion}$ is the volumetric and time-averaged ion density in the in the upstream ionization region and $\zeta_{iz}(T_{e(0)}^{ion})$ is the spatially and time-averaged rate coefficient in the ionization region. Physically, Eq. 11 models the process whereby the neutrals are converted to ions as they traverse the ionization zone. This process is moderated by collisions with ion density (which scales with discharge current in our approximation). There is an explicit time delay associated with this process, which stems from the finite time, $\tau_n$, neutrals require to traverse the upstream zone. This delay is the type of mechanism we showed in the preceding section is necessary to explain the neutral dynamics in the acceleration zone.

With this in mind, we substitute Eq. 11 for flux into Eq. 10 to find

$$\frac{d\langle n_n\rangle}{dt} = \delta_1\frac{\dot{m}}{m_i}\frac{1}{AL}\exp\left[-\frac{1}{I_0}n_{i(0)}^{ion}\zeta_{iz}(T_{e(0)}^{ion})\int_{t-\tau_n}^{t} Idt\right] - \delta_2 n_{i(0)}\langle n_n\rangle\frac{I}{I_0}\zeta_{iz}(T_{e(0)}), \tag{12}$$

To evaluate the validity of this expression, we assume an electron temperature in the ionization region of $T_{e(0)}^{ion} = 5$ eV and an ion density that corresponds to an assumed total axial drift of ions and electrons in this region approaching the Bohm speed $u_i - u_e \approx c_s$ This is commensurate with the assumption that this region is correlated with the pre-sheath of the anode. For our average discharge current of $I_0 = 10$ A, we thus find $n_{i(0)}^{ion} \approx 3.6\times10^{18}$ m$^{-3}$. For the neutral residence time, we assume $\tau_n = 25$ $\mu$s. This corresponds to an approximate ionization region length of 5 mm for a neutral speed of $u_n = 200$ m/s. With these values, we plot the left and right sides of Eq 12 in Fig. 7 where we again note that we adjusted the geometry parameters, $\delta_1, \delta_2$, to find the best agreement. From this result, we can see that this form of the inlet flux is sufficient to describe the discharge current oscillations.

*5. Summary*

In summary, in this section we have employed our experimental observations to justify several simplifications to arrive at two governing quasi-0D equations, Eqs. 8 and 12, for the evolution of the discharge current and neutral density in the acceleration zone. These equations in practice are identical to the model originally proposed by Barral and Peradzyński [11]. The nomenclature “quasi" reflects the fact that these governing equations effectively model two 0D zones.

Physically, Eq. 11 combined with Eqs. 8 and 12 lends itself to the following interpretation. The oscillations in discharge current are driven by the interplay of ionization and electric acceleration in the ionization zone (Eq. 8). These current fluctuations are communicated upstream instantaneously to the ionization region (Fig. 2a) where the changing current impacts the ionization rate of neutrals in this region. The resulting perturbations in neutral density require some

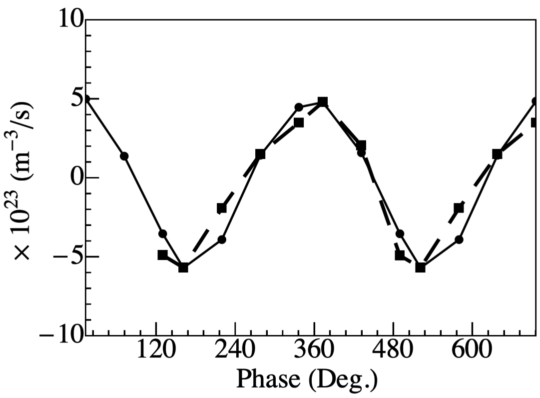


**Fig. 7 Comparison of the derivative of discharge current (solid) with the right side of Eq. 12. The best fit parameters are** $(\delta_1, \delta_2) = (5.8, 1.9)$**.**

.

time to reach the acceleration zone where they can either reinforce or interfere with the on-going oscillations. We expand on this interpretation in Sec. VI

While we have shown that these governing relations can effectively describe the measured oscillations in discharge current and neutral density, we qualify this result with the fact that we have only used one operating condition, 300 V and 10 A, to guide this investigation. This begs the question about the extensibility of this model. One of our ensuring goals thus will be to validate the predictions of this model by parametrically comparing it to thruster oscillations over a wide range of operating conditions. To this end, we turn in the next section to expressing the quasi-0Dmodel in terms of control parameters, e.g. discharge voltage and current, for a Hall thruster.

### E. Expressing governing equations in terms of thruster operating parameters

To perform a parametric comparison of the model to measurements of oscillations in a Hall thruster, we invoke a number of simplifying assumptions to express Eqs. 8 and 12 in terms of common Hall thruster control parameters. These assumptions include

- It has been found empirically that the average electron temperature in the channel of Hall thrusters is approximately 10% of the discharge voltage, [40], $T_{e(0)} = 0.1V_d$. We use this in lieu of solving an energy equation in the plasma.
- The average contribution to ion current in the channel can be related to the total discharge current through the beam utilization efficiency $I_i = qn_{i(0)}Au_{i(0)} = \eta_b I_0$ where $\eta_b$ is the beam utilization efficiency that is typically $\sim 75 - 90\%$ [42]. We thus have $n_{i(0)} = \eta_b I_0/(qAu_{i(0)})$
- The average ion velocity in the channel is the average of the exhaust velocity and zero such that $u_{i(0)} = 0.5\sqrt{2qV_d/m_i}$.
- The average combined ion and electron drift in the upstream ionization region is on the order of the Bohm speed, e.g. $u_i - u_e \approx c_s^{ion}$. This is driven by the fact that the near anode region supports a pre-sheath. This assumption thus yields $n_{i(0)}^{ion}/I_0 = 1/(qA\sqrt{qT_{e(0)}^{ion}/m_i})$
- Since the electron temperature decreases from the acceleration region to the ionization zone, we approximate the average electron temperature in the ionization region as the average between the acceleration zone and zero. This yields $T_{e(0)}^{ion} \approx 0.05V_d$.
- The plasma is primarily singly-ionized with nearly 100% mass utilization. We therefore can relate mean discharge current and mass flow rate, $\dot{m}_i/m_i = \eta_b I_0/q$.

Subject to these simplifying assumptions, we can re-write Eqs. 8 and 12 as

$$\frac{dI}{dt} = I\zeta_{iz}(0.1V_d)\left[n_n - n_{n(0)}\right]$$
$$\frac{dn_n}{dt} = \frac{\eta_b I_0}{q}\frac{1}{AL}\exp\left[-\frac{\zeta_{iz}(0.05V_d)}{qA\sqrt{q0.05V_d/m_i}}\int_{t-\tau_n}^{t} I dt\right] - n_n I \frac{1}{qA0.5\sqrt{2qV_d/m_i}}\zeta_{iz}(0.1V_d). \tag{13}$$

Here we have eliminated the notation $\langle .. \rangle$, instead recognizing that $n_n$ in this equation corresponds to the actual volumetric average. Indeed, we no longer need to apply the geometric correction factors as we did in the preceding section since we are not attempting to compare the solution for neutral density directly to centerline measurements. Rather, our goal will be to use the solution from these equations for discharge current as this is a property of the thruster we can easily assess. To this end, in the next section we will attempt to determine if there are values of the two free parameters of the model, $\tau_n$ and $\eta_b$, for which our model yields predictions for discharge current oscillations that are consistent with experimental measurements for multiple operating conditions.

## III. Experimental setup

For our experimental campaign, we measure parametrically the frequency spectra and amplitude of discharge current oscillations in a magnetically shielded Hall thruster over a wide range of voltage and discharge current. Our overarching goal is to compare the transition points to instability with the theory motivated in the previous section. We in turn use the validated simplified model to guide mitigation strategies. With this in mind, we describe in the following the thruster, the facility, and the key diagnostics and metrics.

### A. Thruster

We employed the H9 Hall effect thruster for this investigation (Fig. 8) [43, 44]. This laboratory thruster was jointly designed by the Jet Propulsion Laboratory, University of Michigan, and the Air Force Research Laboratory and shares design heritage with the Hall Effect Rocket with Magnetic Shielding (HERMeS) developed by NASA in support of the Artemis program. It is nominally a 9-kW class device capable of operation from $V_d = 300 - 800$ V with discharge currents ranging from $I_0 = 5 - 20$ A. The system employs a boron nitride discharge chamber, a centrally-mounted LaB6 hollow cathode, and a magnetically shielded topology. The H9's operation has been characterized extensively on xenon and krypton with previous reported data including both performance and internal plasma measurements [35, 38, 42, 45–48]. For the tests reported in this study, we varied the discharge voltage and current while maintaining the same magnetic field strength. This was accomplished by controlling the mass flow rate through the anode. The flow to the cathode remained at 7% of the anode flow over the range of operating conditions.

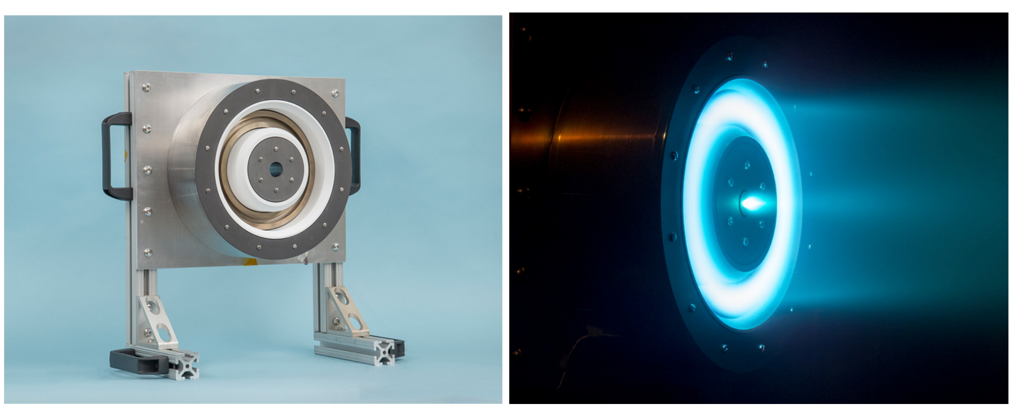

**(a)** **(b)**

**Fig. 8 Images of the H9 Hall effect thruster.**

.

## B. Facility

We performed our tests in the Large Vacuum Test Facility (LVTF) at the University of Michigan [49]. This is a 6 m × 9 m steel vacuum chamber that employs 19 cryogenic pumps to achieve pumping speeds of xenon of 550 kl/s. For this campaign, we measured the background pressure with an ion gauge mounted in the exit plane of the thruster approximately 1 m from the thruster's outer diameter, per the best practice recommendations [50]. For the maximum flow rates in this campaign, $\sim$ 150 sccm of xenon, the facility pressure did not exceed 5 $\times 10^{-6}$ Torr.

LVTF is equipped with power supplies, flow manifold, and telemetry systems for controlling and monitoring thruster health. For this campaign, the discharge power was provided by a 150 kW, 1000 V Magna power supply. This was placed in series with a filter circuit to protect the supply from large scale transients. This consisted of an RLC circuit comprised of a 100 Ohm resistor, 47 uF capacitor, and 0.3 mH inductor. Power to the thruster's electromagnets was provided by a series of TDK lambda power supplies. The thruster flow was controlled by a series of calibrated Alicat flow controllers. The thruster's operation and health were controlled and monitored with an optically-isolated telemetry system that logged measurements of key data including the DC discharge voltage, flow rate, and DC discharge current.

## C. High-speed current probe

The primary diagnostic we employed for this campaign was a high-speed current gun connected to the anode side of the discharge supply line. We also monitored the cathode line current as well as the voltage applied to the thruster. These showed quantitative agreement with the anode line in terms of relative amplitude and frequency of oscillations. For brevity, we do not report these latter measurements here. For all cases, the sampling rate was 625 kHz with 62 kilosamples.

# IV. Results of parametric study and comparison to model

We present in this section the properties of the discharge current oscillations in the H9 thruster as a function of operating condition. We in turn compare these properties to the prediction of the quasi-0D model. To this end, we first show comparisons of power spectra and time-resolved oscillations at a high voltage (specific impulse) condition. We then expand the study to include a parametric study over a wide range of voltages and currents.

## A. Mode transition at 600V

Fig. 9 exhibits the time-dependent variations in current and the power spectra for two discharge currents, $I_0$ = 7.5 A and $I_0$ = 15 A, at a discharge voltage of $V_d$ = 60 V. As can be seen, at $I_0 = 7.5A$, the thruster exhibits a coherent and large amplitude ( $>$ 100% of the mean value) with a fundamental frequency of 15 kHz. The harmonics in the spectra above 15 kHz indicate the cnoidal nature of the oscillation. This low frequency oscillation is typical of the canonical breathing mode oscillation [4]. At the higher discharge current, $I_d$ = 15 A, the power spectrum still exhibits a peak at 15 kHz, which is commensurate with the breathing mode, but the amplitude is six orders of magnitude smaller. This is too low to be observed in the time-resolved signal. With that said, the current does still oscillate but with a dominant frequency of 70 kHz and an amplitude that is an order of magnitude lower than the breathing mode amplitude at $I_0$ = 7.5 A. This higher frequency instability is fundamentally different than the breathing mode and has been shown in magnetically shielded thrusters to be associated with a rotational cathode mode [32, 47, 51]. In summary, these results show that with increasing current, the breathing mode is damped and higher frequency oscillations can dominates the discharge.

For comparison to these experimental results, we show the predictions for the discharge current oscillations per Eq. 13. To solve these governing equations numerically, we assumed a beam utilization efficiency of $\eta_b$ = 75% (typical of Hall thrusters [40]) and a neutral residence time of $\tau_n$ = 22 $\mu$s. We note here that we found that the numerical solutions of these equations always converged to the same cycle regardless of initial conditions. This is a physical reflection of the fact that there is a dominant, spontaneously mode represented by these equations. With this in mind, we show in Fig. 9 the mode solutions for the two discharge currents as well as the Fourier spectra of these solutions. It is evident from this figure that the quasi-0D model, when tuned in terms of its free parameters, is able to capture the time-resolved and spectral properties of the large scale oscillation at $I_0$ = 7.5 A. Similarly, at $I_0$ = 15 A, the model correctly recreates the effective damping of the breathing mode. This is represented by the non-oscillatory current and the absence of spectral content in the power spectrum. We note, of course, that the model does not re-create the higher frequency oscillation exhibited by the experimental data at $I_0$ = 15 A, as the underlying physics of this simple model cannot represent the rotational cathode mode. With that said, at least in terms of representing the thruster dynamics for

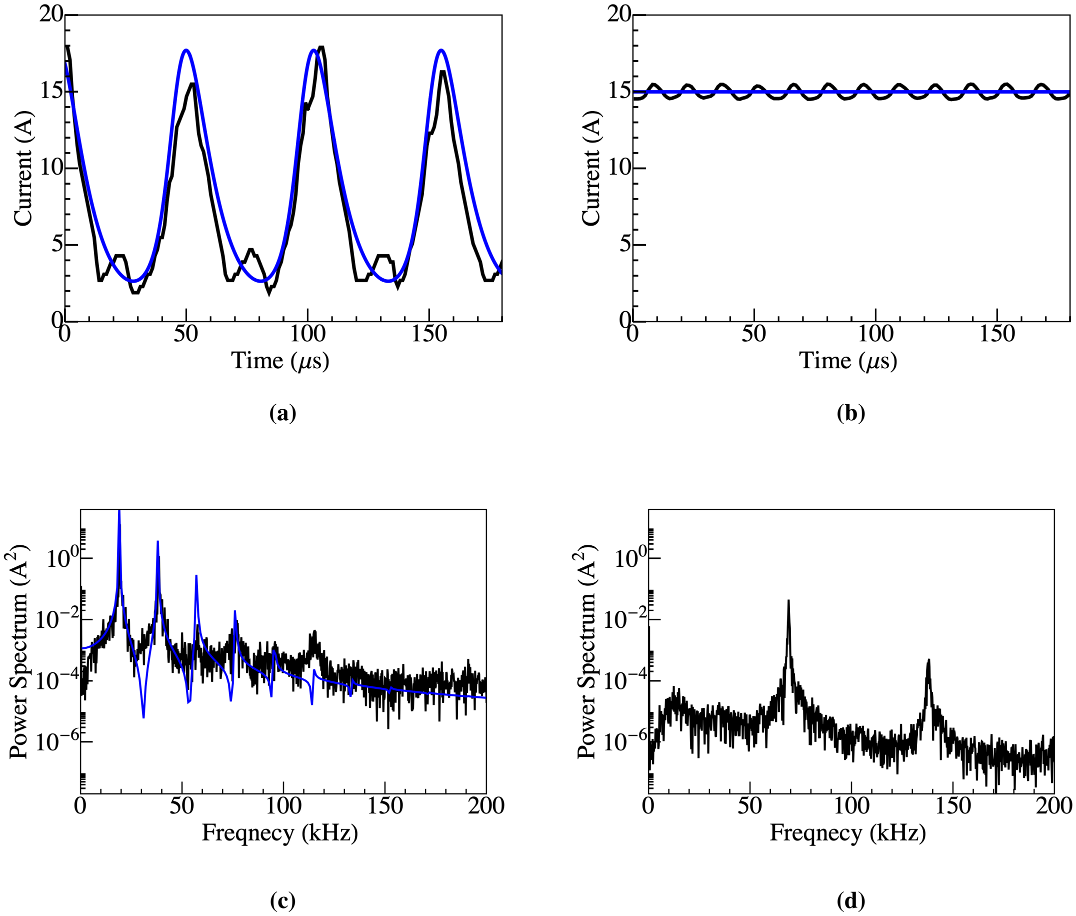


**Fig. 9 a) Comparison of experimental measurement (black) and model (blue) for current oscillations in time at a) $V_d$ = 600 V and $I_0$ = 7.5 A and b) $V_d$ = 600 V and $I_0$ = 15 A. Power spectra at c) $V_d$ = 600 V and $I_0$ = 7.5 A and d) $V_d$ = 600 V and $I_0$ = 15 A. The model result for the power spectrum is not shown for (d) as the oscillation level is negligible at this level. Best fit parameters for the moel are $\eta_b$ = 0.75 and $\tau_n$ = 22 $\mu$s.**

.

the mode transition of the breathing mode oscillation at 600 V, this is a preliminary validation of the model's predictive capability.

### B. Parametric study over operating conditions

To expand on the results from the previous section, we consider in this section the dependence of the oscillation properties parametrically on operating condition. To this end, we invoke two global metrics for representing the oscillation properties. The first is the average relative peak-to-peak amplitude of the fluctuation, RPK. To evaluate this parameter, we divide both the experimental and model time-resolved data into $N$ time series of length $\Delta t \sim 200$ $\mu$s. We then define

$$\mathrm{RPK} = \frac{100}{N}\frac{\sum_{j=1}^{N}\left(I_{max(j)} - I_{min(j)}\right)}{I_0}, \tag{14}$$

where $I_{max(j)}$ and $I_{min(j)}$ denote the maximum and minimum of the current oscillation in the $j^{th}$ time series. This figure of merit indicates the magnitude of the strength of oscillation. The second metric we employ is the frequency of the dominant oscillation, $f_{max}$. This is extracted from the Fourier transform. As we have noted in the preceding section (Fig. 9), there are experimental configurations in which the dominant oscillation is not the breathing mode but rather a higher frequency oscillation that is not modeled by the quasi-0D theory. In this case, we identify the frequency consistent with the lower amplitude peak close to the breathing mode frequency and identify this as $f_{BM}$.

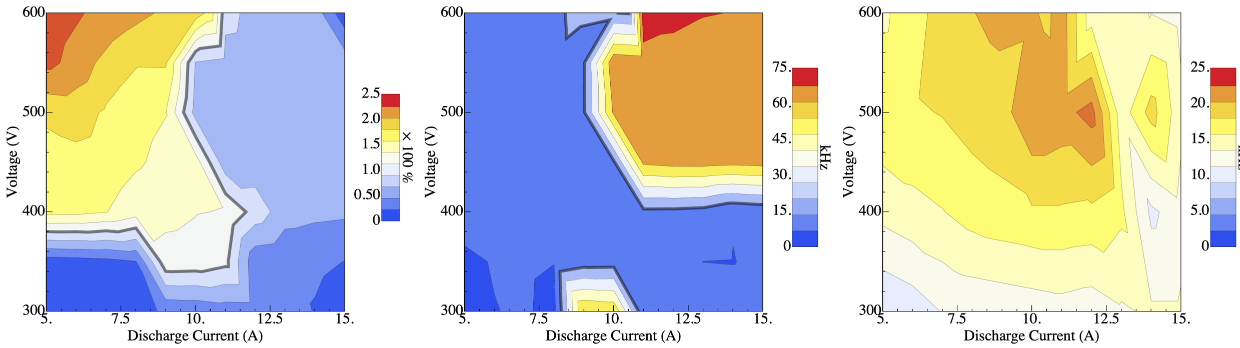


**(a)** **(b)** **(c)**

**Fig. 10 a) Relative peak-to-peak in discharge current oscillation level, b) dominant frequency of discharge current oscillation, c) frequency of the oscillation associated with the breathing mode. The bolded contour on (a) denotes the 100% fluctuation level while in (b) it denotes the mode transition in frequency. Linear interpolation is employed to generate this figure.**

.

*1. Experimental results*

We show in Fig. 10 the measured relative peak-peak to amplitude of oscillation as a function of discharge voltage and current. We generated this result by controlling the thruster to each operating each condition and waiting until the mean discharge current, $I_0$, achieved a steady-state value. We then recorded the time-resolved discharge current. The voltage resolution of this map is 50 V while the current resolution is in 1 A increments.

The compiled result shows that at fixed voltages above $V_d$ = 400 V, there is a range of discharge currents, $I_0 = 10 - 12$ A, below which the thruster transitions from a region of low oscillation amplitude (RPK < 50%) to high amplitude (RPK > 100%). This transition is consistent with the result shown in Fig. 9a. Below 350 V, however, a transition to instability does not onset for the range of currents interrogated.

We note here that in departure from our analysis in Sec. II where we analyzed the high amplitude oscillations at $V_d$ = 300 V and $I_0$ = 10 A to guide our model development, Fig. 10a shows this condition is relatively quiescent. This difference can be ascribed to the fact that we employed a different, off-nominal magnetic field strength for the study performed in Ref. [38] that formed the basis of the data reported in Sec. II. In this former case, we deliberately adjusted the magnetic field to achieve an oscillatory state. This was to facilitate the diagnostic technique. In the study reported here, we have employed a magnetic field 25% stronger, which evidently allowed for more stability at this operating condition. We return to a discussion of the role of the magnetic field in the following section.

We show in Fig. 10b the dominant frequency, $f_{max}$, from the power spectra of the discharge current oscillations. This result shows a transition from highly oscillatory conditions dominated by the lower, breathing mode frequency ($f_{max} \approx 10 - 20$ kHz) to a state exhibiting the higher frequency cathode oscillation, $f_{max} \approx 70$ kHz. This transition in the dominant frequency mirrors the trends in the RPK amplitude oscillations (Fig. 10a) and thus provides additional confirmation of the mode transition in the thruster. Most saliently, the RPK = 100% contour in Fig. 10a approximately follows the contour in Fig. 10b where there is an evident shift in frequency. In our subsequent analysis with our model, we thus use the value RPK = 100% as the criterion to denote a mode transition. This threshold is marked by the bolded contour line in Fig. 10a.

As a final metric, we show in Fig. 10c the frequency of the breathing mode frequency, $f_{BM}$, for all oscillating conditions, recalling that this mode persists but with a several order of magnitude decrease in amplitude (c.f. Fig. 9). This result suggests that for currents below $I_0 = 12.5A$, the breathing mode frequency increases with both voltage and current. However, the relative change in magnitude is small, with frequencies ranging from $\sim$ 10 kHz at the lower end of the parameter space to 19 kHz at the upper end. Beyond $I_0$ = 12.5 A, the trends are not as immediately evident, but this may in part be attributed to the fact that the breathing mode is largely damped at these higher currents and poorly defined. Indeed, the frequency peak associated with the lower frequency mode becomes progressively broader as the

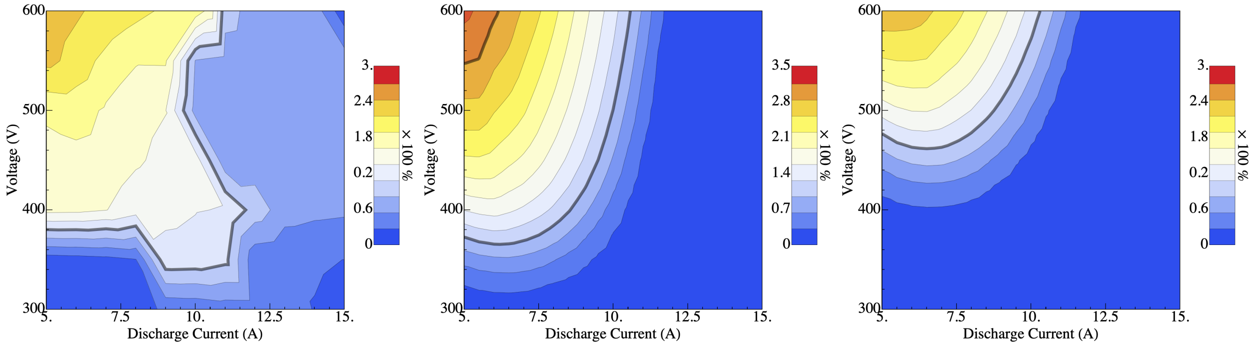


**(a)** **(b)** **(c)**

**Fig. 11 Relative peak-to-peak in discharge current oscillation level from a) experimental measurement, b) quasi-0D model with $\tau_n = 19$ $\mu$s and $\eta_b = 90\%$, and c) quasi-0D model with $\tau_n = 16$ $\mu$s and $\eta_b = 90\%$. The bolded contour denotes the 100% line for all three cases.**

cathode oscillation becomes more prevalent at higher currents.

### *2. Comarisont to model*

We next employ our quasi–D model for comparison with these experimental measurements. To generate these results, we parametrically explored different combinations of neutral transit time and beam utilization to find the best quantitative match with the data. This was accomplished through empirical iteration and not with a formal minimization scheme. Through this process, we show the experimental values in Fig. 11a compared to the model for two cases of fit parameters: $\tau = 19\mu$ s and $\eta_b = 90\%$ in Fig. 11a and $\tau = 16\mu$ s and $\eta_b = 90\%$ in Fig. 11c. Note that these are different values than those we employed in Fig. 9. This is a result of the fact that in this case, our goal was to match global trends in parameter space rather than those at just a single fixed voltage. This speaks to the larger point that these model parameters likely are not constant for all parameter space. By using fixed values in this section, we thus are explicitly assuming “average" values over the domain. We return to this point in Sec. VI. Significantly, $\eta_b = 90\%$ is actually in line with previous experimental measurements of the H9 Hall thruster [42].

With said, in all three plots in Fig. 11, we have adopted the same color scheme and denoted with a bolded line the contour correspond to RPK = 100%. It is evident from this result that for both sets of fit parameter, the simplified model is able to capture qualitatively the trends in RPK with voltage and current. At fixed voltage, there is a characteristic value of current where the oscillation levels shifts from low amplitude to high. Similarly, the value where this transition occurs appears to depend on voltage in a qualitatively similar way.

Case Fig. 11(b) shows the better agreement of the two modeling results with the data, though there is an exception below $V_d = 350$ V where the experimental results show a non-monotonic change in the RPK = 100% demarcation line. The reason for this departure between model and experiment here is not immediately evident, though we note that this is a region in parameter space where we have observed comparable amplitude in cathode and breathing mode oscillations experimentally. This may in part obscure the transition. To this point, as we discussed in the context of Fig. 9, the model predicts zero-amplitude oscillations for sufficiently high current and cannot capture the cathode oscillation. This is why the RHS values collapse to zero in the model plots while they remain finite for the experimental case. With that said, we do note that for higher current oscillations, i.e. above the 150% threshold where the breathing mode unambiguously dominates, the shapes of the contours for the model and experiment agree.

As a final note, we remark that the choice of neutral transit time plays a critical role in the stability threshold for the thruster. This speaks to the role of relative transit time of the neutrals in enhancing the instability. We return to this discussion in Sec. VI. In summary, these results suggest that the quasi-0D model, when properly tuned, is able to capture with a high degree of fidelity the trends in amplitude for the breathing mode oscillations in the H9.

Fig. 12 shows a comparison of the frequencies of the breathing mode oscillation compared to the model predictions for the same two sets of fit coefficients as we employd for Fig. 11. In this case, we that the model that yielded the best agreement for amplitude of oscillations, 11b, does not exhibit the same degree of agreement for trends in frequency. Overall, the frequency of oscillation for most of the parameter space is higher than measurement and does not show the same degree of variation. With that said, we note that the frequencies do only differ by a factor of 25% for most of the domain. This suggests at least qualitatively that the dynamics of the underlying timescales are approximately correct. Fig. 12c shows improved agreement in qualitative trends with the experimental measurements. Indeed, even the feature where there is a decrease in frequency for currents above $I_d = 12.5$ A is captured. As with Fig. 12b, the magnitude of the frequency remains too high compared to experimental. The range of oscillations similarly is too narrow. However, the ability to represent at least qualitatively the trends in frequency with operating condition is an encouraging initial result–particularly in light of the several simplifying assumptions we employed in our analysis. Indeed, potentially, with additional and more rigorous regression, even better agreement across cases may be found.

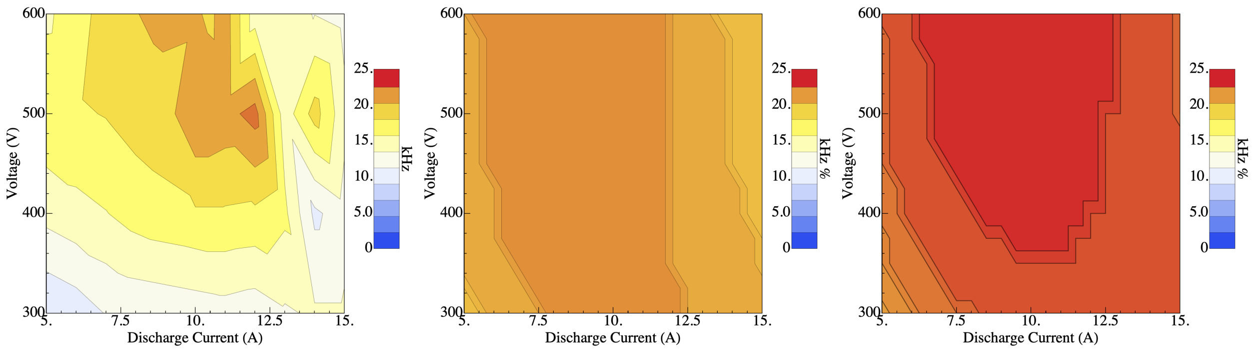


**(a)** **(b)** **(c)**

**Fig. 12 Breathing mode oscillation frequency for a) experimental measurement, b) quasi-0D model with $\tau_n = 19$ $\mu$s and $\eta_b = 90\%$, and c) quasi-0D model with $\tau_n = 16$ $\mu$s and $\eta_b = 90\%$. The bolded contour denotes the 100% line for all three cases**

In summary, the ability of this simplified mode to represent key trends in frequency and oscillation amplitude suggests that it may be capturing key elements of the physical processes governing the mode transition in the thruster. We discuss in more detail in Sec. VI the physical underlying this transition. However, for the purpose of exploring mitigation, we take this initial validation as an encouraging result to identify strategies to mitigate the transition.

## V. Approach to mitigation

Based on the conclusion that the model can re-create key trends for the mode transition in the H9, we turn in this section to leveraging the quadi-0D model to identify strategies to try to mitigate the mode transition. The overarching goal in this case, driven by the mission application discussed in Sec. I, is to operate the thruster at low discharge current ($I_0 < 10$ A) while maintaining higher discharge voltage (e.g. $V_d = 600$ V). To this end, we first non-dimensionalize the governing equations in an effort to find an analytical expression for stability criterion. We then employ this relation to identify possible strategies for mitigation. These finally are tested through a set of proof-of-concept experiments.

### A. Derivation of stability criteria

To arrive at an analytical stability criterion for the mode transition, the standard approach is to linearize the governing equations and to search for solutions in complex space with positive imaginary components We note, however, that the dynamics of the oscillations when they onset are evidently non-linear. This was a potential issue as noted by Barral as well [11]. In order to find a stability criterion then for these non-linear oscillations, we adopt an alternative, semi-empirical approach.

To this end, we first non-dimensionalize the governing equations in Eq. 13 by invoking the following non-dimensional relations:

$$\bar{t} = t n_{n(0)} \zeta_{iz}(T_{e(0)}) \qquad \bar{n}_n = \frac{n_n}{n_{n(0)}} \qquad \bar{I} = \frac{I}{I_0}\alpha_{iz}. \tag{15}$$

In this first relation, we have normalized the time by the average ionization frequency in the acceleration zone. In the second element, we have normalized the neutral density in the acceleration zone by the average value. In the third relation, we have normalized the discharge current by the time-average discharge current scaled by the ionization fraction in the acceleration zone, $\alpha_{iz} = n_{i(0)}/n_{n(0)}$. Armed with these definitions, we can re-write Eq. 13 as

$$\frac{d\bar{I}}{d\bar{t}} = \bar{I}\left(\bar{n}_n - 1\right) \tag{16}$$

$$\frac{d\bar{n}_n}{d\bar{t}} = \bar{I}_0 \exp\left[-\Gamma\left(\int_{\bar{t}-\bar{\tau}_n}^{\bar{t}} \bar{I} d\bar{t} - \bar{\tau}_n \bar{I}_0\right)\right] - \bar{I}\bar{n}_n, \tag{17}$$

where we have defined $\bar{I}_0$ as the normalized average current and $\bar{\tau}_n = \tau_n n_{n(0)} \zeta_{iz}(T_{e(0)})$ as the normalized neutral transit time. We also have introduced the term $\Gamma = u_{i(acc)}/u_{i(ion)} \left(\zeta_{iz}(T_e^{ion})/\zeta_{iz}(T_{e(0)})\right)$. For the simplifying assumptions we have made for the scaling of electron temperature and acceleration zone, this paramter is a weak function of voltage—over the range of $V_d = 300 - 600$ V it varies from 0.6 to 0.75. We therefore approximate $\Gamma \approx 0.68$ as a constant. In so doing, we thus have rendered Eq. 17 into a set of governing equations that only depends on two free parameters, the normalized neutral transit time, $\bar{\tau}_n$, and the normalized average discharge current, $\bar{I}_0$. With this in mind, we can evaluate this governing equation over a range of anticipated normalized values to search for trends in the stability threshold.

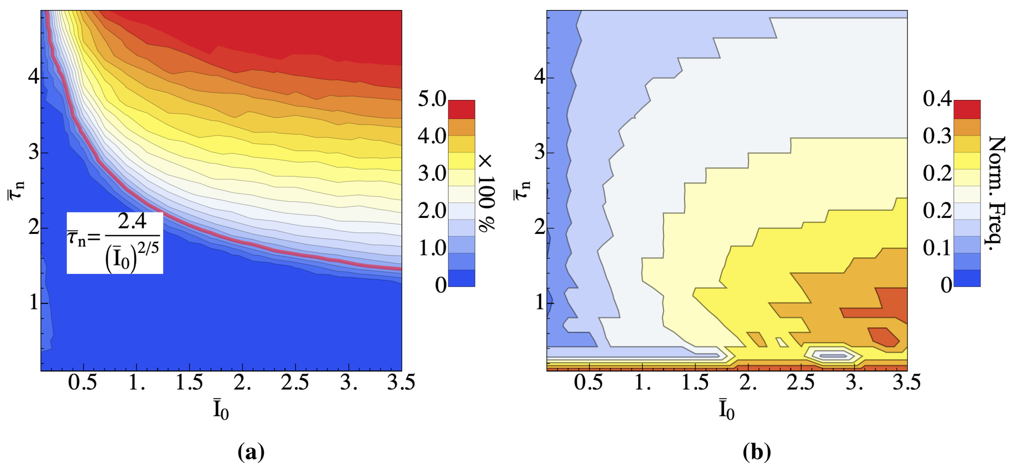


**Fig. 13 a) Average relative peak-to-peak oscillation and b) normalized frequency from solutions to normalized governing equations, Eq. 17, as a function of normalized current and neutral transit time. The red curve corresponds to the 100% contour.** $\Gamma = 0.68$ **for these results.**

For our operating conditions of the H9 and subject to the simplifying assumptions we made in Sec. II.D, we anticipate ranges of the normalized parameters of $\bar{\tau}_n \epsilon (1, 5)$ and $\bar{I}_0 \epsilon (0.5, 3.5)$. For this range of values, we show in Fig. 13 the RPK and peak normalized frequencies from the solution to Eq. 17 with $\Gamma = 0.68$. The key features from Fig. 13a are the well-defined contours, which represent constant peak-peak amplitude oscillation as a function of the normalized parameters. We can leverage these contours to arrive at a stability threshold from this result. In particular, we select the trend that corresponds to 100% peak-to-peak oscillations (denoted by a red line in Fig. 13). By inspection, we then can fit a curve to this contour to yield a stability criterion:

$$\bar{\tau}_n > \frac{2.4}{\bar{I}_0^{2/5}}. \tag{18}$$

This in turn yields

$$\bar{\tau}_n^{5/2} \bar{I}_0 > 8.9. \tag{19}$$

As a last step, we can convert this result to an expression that depends on operating condition by removing the normalization. This yields

$$\frac{I_0 \zeta_{iz}(0.1V_d)}{qA} \left(\frac{\eta_b^3 (0.5\sqrt{2qV/m_i}) \tau_n^5}{L^3}\right)^{1/2} \exp\left[-\frac{3}{2}\frac{I_0}{qA}\frac{\tau_n \zeta_{iz}(0.05V_d)}{\sqrt{q 0.05 V_d/m_i}}\right] > 8.9. \tag{20}$$

In principle, this criterion is general over all operating conditions of interest for our system. We thus can leverage it to motivate mitigation strategies for moving the discharge current where the mode transition occurs. Most relevantly, we see that there are two parameters that we can control with our current setup: the beam utilization efficiency, $\eta_b$, and the neutral transit time, $\tau_n$. For a fixed discharge voltage, e.g. $V_d$ = 600 V, these relations in turn suggest that the stability threshold can be shifted to lower currents by either reducing the beam utilization efficiency or decreasing the neutral density resident time. The physical reasons underpinning this control are that both of these parameters impact the ionization rate in the ionization zone and therefore influence the feedback process driving the mode unstable. We return to this physical interpretation in Sec. VI.

### B. Frequency of breathing mode oscillation

We show in Fig. 13b the normalized frequency of the peak oscillation from the solutions to Eq. 17. While this plot shows evident trends in the variation of this parameter, the relative changes are modest—from 0.1-0.3 over the domain. As an approximate scaling law, we therefore make the simplification that the predicted normalized frequency is approximately constant. We thus find in dimensional terms

$$f_{BM} \approx 0.15 n_{n(0)} \zeta_{iz}(0.01 V_d). \tag{21}$$

This expression suggests that the predicted frequency is on the order of the ionization frequency inside the accceleration zone. This is broadly consistent with previous analyses of the breathing mode oscillation [6]. To relate this result to the operational parameters, we invoke the steady-state expression for neutral density in the acceleration zone to find

$$f_{BM} \approx 0.15 \exp\left[-\frac{I_0 \tau_n \zeta_{iz}(0.05 V_d)}{Aq\sqrt{2q0.05V_d/m_i}}\right] \frac{\eta_b 0.5\sqrt{2q0.1V_d/m_i}}{L}. \tag{22}$$

This relation quantifies how both the voltage and current impact the predicted frequency of the breathing mode oscillation in a shielded thruster.

### C. Impact of magnetic field strength

Adjusting the magnetic field, $B_0$, is one of the most common approaches to controlling the oscillation level in Hall thrusters [29, 32, 52]. This dependence, however, is not always monotonic, and can in fact exhibit minima in oscillation level. In the context of Eq. 20, this dependence can in part by understood from the relationship of beam utilization efficiency to magnetic field magnitude, $\eta_b(B_0)$. In principle, larger magnetic fields constrict cross-field electron flow, thereby raising this efficiency. For a fixed discharge voltage, this would suggest from the scaling in Eq 20 that increasing magnetic field will shift the discharge current where the instability transition occurs to higher values. The strategy for moving the instability margin to lower currents therefore would be to lower the magnetic field. With that said, the adjusted magnetic field also can impact other background properties like electron temperature, $T_e(B_0)$ and the effective length of the acceleration zone, $L(B_0)$. This underscores a major limitation with the simple formulation we have described in Eq. 20 in that we do not a priori have the ability to determine this dependence—we instead have adopted rules of thumb (e.g. the 10% scaling of temperature with voltage).

With that said, assuming that at least for minor relative changes in magnetic field the dominant impact is on the beam utilization, we can predict how incremental changes may impact the threshold by assuming

$$\eta_b(B_0) \approx \eta_{b(nom)} \frac{B_0}{B_{nom}}, \tag{23}$$

where $B_{nom}$ is the nominal magnetic field strength that we used during our parametric study. With this in mind, we show in Fig. 14a the predictions for the 600 V case for the relative peak to peak oscillations as a function of discharge current for different magnetic field strengths. This figure suggests the transition point to instability should move to lower currents with lower magnetic field.

To evaluate this mitigation method experimentally, we repeated the stability study on the H9 thruster at 600 V as a function of current at different applied magnetic field strengths. Fig. 14 shows these results compared to our stability predictions. We note that unlike the quasi-D model in which the oscillation level is zero above a threshold current, the same is not valid for experiments. As we discussed in the preceding, this stems from the fact that there are still cathode related oscillations in the discharge even when the breathing mode is suppressed. The more salient feature for comparison with our previous criteria is the point where 100% fluctuations occur. This is marked by a horizontal dashed line in the figure. We evidently see that with decreasing magnetic field strength from nominal, the trends in experimental data are consistent with the model predictions. The transition point does move to lower discharge current—by approximately $\Delta I_d = 1.5$ A— consistent with the model prediction. This indicates it is possible to control the onset of the mode.

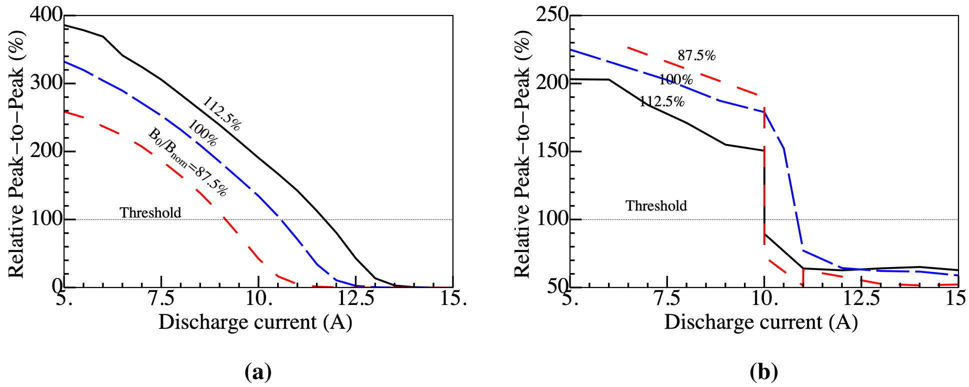


**Fig. 14 Comparison of the a) model predictions and b) experimental measurements of the oscillation amplitude as a function of discharge current for different magnetic field settings. Discharge voltage is $V_d = 600$ V for all conditions. The horizontal dashed line denotes threshold for mode transition.**

On the other hand, we see that experimentally with higher magnetic field strength, the transition point also shifts to lower discharge current. This is counter to the predictions from our quasi-0D model. The underlying reason why the model captures the trends with increasing magnetic field is not immediately apparent from our formulation, but as we discussed in the preceding, it may in part be attributed to the unknown dependencies for electron temperature $T_e(B_0)$ and acceleration zone, $L(B_0)$, not included in our derivation.

### D. Impact of anode temperature

The formulation in Eq. 20 suggests another potential strategy for modifying the transition to instability: adjusting the neutral transition time, $\tau_n$. The reason for this dependence stems physically from the fact that changing the neutral transit time impacts the degree of ionization and thus timing of the feedback from the ionization zone to the acceleration zone. We see in fact from Eq. 20 that the dependence on transit time is non-monotonic—a point we return to in the discussion. With that said, for minor changes in transition time with respect to best fit parameters we have identified to the experimental data in Fig. 11, our stability criterion suggests that decreasing $\tau_n$ will lead to a lower current where the transition in stability occurs.

With this in mind, the neutral transit time in principle can be by controlled by adjusting the anode temperature [53]. The neutrals emerge from anode at equilibrium with this electrode. Hotter temperatures therefore correspond to faster neutrals. Since the neutral transit time in the ionization regime is inversely proportional to neutral speed, a hotter anode thus will correspond to smaller values of $\tau_n$. To illustrate the predicted implications of this change, we show in Fig. 15a the peak-peak relative oscillations as a function of current for the $\tau_n = 19$ $\mu$s we determined from the best fit to our data, and we show the trends for $\tau_n = 17$ $\mu$s, which could correspond to an approximately 20% increase in anode temperature. This result shows that this change in transit time can in theory move the mode transition to lower currents.

To assess the implications of this change experimentally, we again employed the H9 thruster where we performed a stability study at the maximum voltage, $V_d = 600$ V, as a function of discharge current. In order to increase the anode temperature, we ran the thruster at its maximum power condition, $V_d = 600$ V and $I_0 = 15$ A, for three hours. We then rapidly decreased the current over 30 s from 15 A to 5 A by lowering the anode flow rate and monitoring the discharge current oscillations with a high-speed data acquisition card. The motivation behind this approach was that the timescale of the ramp down in current would be faster than the thermal equilibration timescale of the thruster. Thus, the anode would remain artificially hot over the current sweep, lowering the effective value of $\tau_n$. We note that this attempt to control temperature was a departure from our initial parametric study in which we only waited at each thruster setting until the anode current had plateaued before proceeding. The thruster was not at thermal steady state at each power for these measurements.

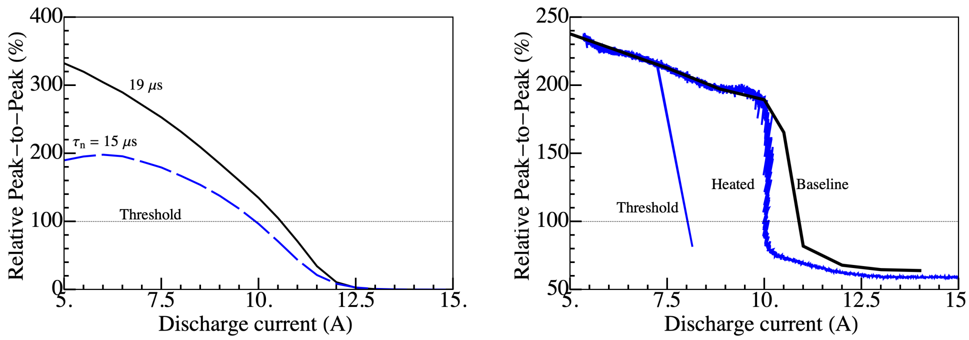


**(a)** **(b)**

**Fig. 15 Comparison of the relative oscillation amplitude for a) model predictions for different neutral transit times and b) experimental measurements for different anode temperatures. Discharge voltage is $V_d = 600$ V for all conditions. The horizontal dashed line denotes threshold for mode transition.**

With that said, we show in Fig. 15b the results of this study where we plot the peak to peak amplitude of oscillations as a function of discharge current for the baseline and heated anode cases. The shift in current is qualitatively consistent with Fig. 15a in which we predicted the transition point would move to lower current. We cannot directly compare the two results as we did not have direct measurements of anode temperature. However, this figure does suggest that adjusting neutral transit time is a possible viable mechanism for controlling the mode transition.

## VI. Discussion

We discuss in the following several aspects of the preceding experimental and numerical work. First, we leverage our normalized stability analysis to provide a physical interpretation of the mechanisms driving the growth of the instability. We then review the assumptions of our model and their impact on model validity. We finally conclude with a discussion of the implications of our results for efforts to mitigate the transition to instability and possible implications for ground testing efforts.

### A. Physical interpretation of model

In our motivation for arriving at the simplified quasi-0D model, we have argued that it was necessary to have an element to introduce positive feedback to reinforce the ionization oscillations in the acceleration zone. This interpretation is consistent with the larger body of work on the breathing mode oscillation where it has been suggested that this mode is inherently more than zero-dimensional [11, 13, 21, 22, 41]. To this end, following Barral [11], we have treated the thruster as two 0D regions where the dominant properties that oscillate on the timescale of the ionization frequency are the discharge current and neutral density. These two 0D regions are causally connected by two processes: 1) the flux of perturbations in the neutrals from the upstream ionization region to the downstream acceleration zone and 2) the changes in discharge current that originate in the acceleration zone that are communicated “instantaneously" (on the timescale of the breathing mode) upstream to the ionization zone. The timing of this relationship is moderated by the neutral transit time through the ionization zone. Ultimately, the ionization promoted by changes to the discharge current in the ionization zone enables a positive feedback loop in variations in neutral density in the acceleration zone. These fluctuations can constructively interfere to promote growth of the instability.

The stability criterion we derived in Eq. 20 reflects this interpretation. Indeed, this result also can be written as

$$\left[\left(\tau_n \nu_{iz(0)}\right) \exp\left[-\frac{3}{2}\nu_{iz(0)}\tau_n\right]\right] \eta_b^{3/2}\Gamma^{1/2}\left(\frac{\tau_n}{\tau_i}\right)^{3/2} > 8.9, \tag{24}$$

where $\nu_{iz(0)}$ denotes the ionization rate of neutrals in the ionization zone and $\tau_i = L/u_{ion}$ is the transit time of ions through the acceleration zone. The term in the brackets in this expression illustrates the dependence on the relative timescale of ionization to transit time. To highlight this, we plot in Fig. 16 this trend for fixed values of $\tau_n$, $\tau_i$, $\Gamma$, and $\eta_b$.

We see from this result that the stability criterion is only satisfied for intermediate values of the ratio of timescales. Physically, if the ionization rate is small compared to the neutral transit time in the ionization region, i.e. $\tau_n \nu_{iz(0)} \ll 1$, the neutral density has only slight modulation in the ionization region before entering the acceleration zone. There is no mechanism for positive feedback in oscillations from the ionization region upstream. Rather, the system converts to the case with a steady influx of density, which is unconditionally stable [41]. On the other hand, if the ionization rate is too high, $\tau_n \nu_{iz(0)} \gg 1$, with respect to the transit time, the neutral density is depleted before entering the ionization zone. There again is no mechanism for oscillations in neutral density to positively couple with fluctuations in the acceleration zone. The mode is stable. It is in the intermediate range of frequency ratio that the oscillation thus will be driven unstable.

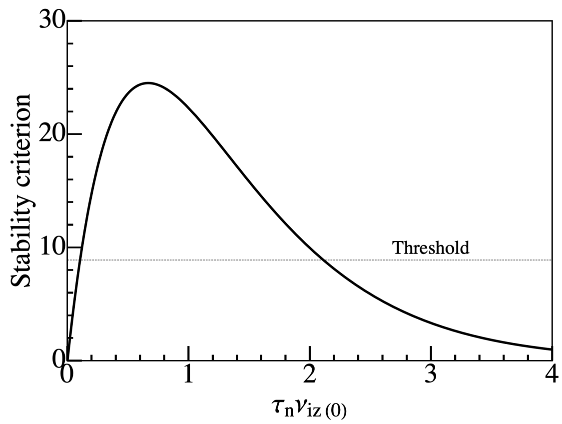


**Fig. 16 Stability criterion from Eq. 24 as a function of the ratio of neutral resident time to ionization timescale in ionization region.**

.

As the effective ionization rate depends on the density of ions, which in turn in our formulation scales with the discharge current, we thus now can understand the dependence on current illustrated by our numerical solutions (Fig. 10). The current is a moderator for the relative ionization frequency compared to timescale of neutral transit. For higher voltages (e.g. $V_d > 350$ V), we see there is an intermediate range of current where instability occurs. This is where the relative ratio of neutral residence time to ionization timescale leads to positive feedback of the instability. Outside of this range, we predict a stable oscillation. This is the range where the discharge current is sufficiently high (or low) that positive feedback does not occur. As voltage increases, the electron temperature and therefore ionization rate increase for a given discharge current. The same level of current thus can have a higher degree of ionization. It is for this reason that we see the range of currents where instability occurs growing wider with increasing voltage.

### B. Validity of assumptions and implications for model

We review here the key assumptions underpinning the model derivation and discuss their implications for the model applicability and extensibility. The key assumptions include

- The plasma can be treated as two 0D regions where the dominant properties that oscillate on the timescale of the ionization frequency are the discharge current and neutral density.
- The dominant contributor to fluctuations in discharge current stems from the variations in plasma density—not fluctuations in the electron and ion drift speeds. This was justified by considering the phase relations among experimental properties in the acceleration zone.
- To relate thruster operation parameters, discharge current and voltage, to the quasi-0D model, we have invoked a series of simple scaling laws for electron energy and electron transport. Specifically, we have assumed the rule of thumb relationship that $T_e \propto V_d$ in the channel and acceleration zones, and we have assumed a known beam utilization efficient, $\eta_b$, to relate ion and electron currents to the total discharge current
- The neutral transit time, $\tau_n$, length of acceleration zone, $L$, and beam utilization efficiency, $\eta_b$, are all assumed to be constant over the investigated parameter space.

These assumptions are highly idealized compared to the operation of a real system. For example, in practice, the anode temperature will vary with thruster total power. Similarly, the beam utilization efficiency is tied to the operating condition. Yet, when properly tuned in terms of neutral resident team and beam utilization, the quasi-0D model appears to capture key trends in the stability margin of the shielded H9 thruster. This may suggest that the dependence of these properties are weak compared to the other factors influencing the stability, i.e. the variations in electron temperature and ionization rate that results from differences in voltage and discharge current. The values we have found for $\eta_b$ and $\tau_n$ that yield the best agreement with data thus can be interpreted as “averages" over the parameters space. With that said, a higher fidelity approach would attempt to capture these dependencies and may yield improved agreement with the data.

We also note here that the model we have presented is predicated on the ability to use a simplified two-equation model for fluctuations. We have justified this simplification by leveraging the previous numerical work of Barral [11, 13] and employing experimental data from one operating condition of one thruster. In practice, however, we do not know if these assumptions about the phasing relationships between different quantities are extensible over the full operating envelope of the thruster. Indeed, since we have neglected higher fidelity models for the momentum and energy transport in the plasma, it is not evident how justifiable these assumptions remain. With that said, the ability to match the experimental trends helps bolster confidence in the simplifications underpinning the model.

As a final comment, we remark that the simplified scaling relations we have employed such as the fixed proportionality between voltage and temperature can be impacted by thruster geometry, wall material, and gas choice. For example, while we have chosen $T_e = 0.1V_d$ in the acceleration zone and $T_e = 0.05V_d$ in the ionization zone, this scaling factor may change. To apply this model to other systems, then, it may be necessary to treat these scaling factors as free parameters that are also tuned to better match the model. In so doing, the threshold for stability also will change depending on the system under investigation.

### C. Implications for thruster testing and mitigation

Our preceding work has shown how neutral transit time may be a critical feature in determining stability of the thruster. This invites practical questions about the role of the thruster thermal state for the oscillation level in any system. For example, it is common in current Hall thrusters to operate the device for several hours at the nominal power condition to outgas the discharge chamber walls. As part of this outgassing process, contaminants (usually water), are released. This is correlated with an artificial increase in average discharge current and is often associated with higher amplitude oscillations. The oscillation level subsequently decreases over time.

With that said, while it is clear that outgassing is correlated with high amplitude breathing mode oscillations, our work suggests a parallel and complementary interpretation. As the thruster is operated, the temperature of the channel and anode increase. As we have shown in the preceding, this will reduce neutral transit time, and for a given operating condition, reduce the amplitude of oscillations. In addition to eliminating contaminants then, it may be the thermal soaking that also helps improve thruster stability during the initial outgassing/burn in time. This dependence on temperature may have implications for transitioning to orbit as well. Indeed, the thermal rejection on orbit may be different than test facilities in such a way that ultimately may lead to steady-state temperatures of the thruster channel and anode that differ from ground test. This in turn may impact the stability margin for a given operating condition in orbit.

As a final note, we remark here about extensions to mitigation strategies to be able to operate at the targeted condition of high specific impulse (voltage) and low power. Indeed, preliminarily we have shown that changing the thermal environment and magnetic field strength can shift the transition point. Taken to an extreme, we might anticipate that operating a thruster designed deliberately to have an extremely hot anode may exhibit better stability properties at lower current and high discharge voltage. The practical implementation of this approach, of course, may be a major engineering challenge.

There may be other possible strategies as well-informed by the modeling results. For example, we have seen that one way to adjust the stability margin is to reduce the degree of steady-state ionization in the upstream ionization zone (Fig. 16). This could be accomplished, for example, by lowering the electron temperature in this region. Indeed, we have found that if we assume the scaling with voltage in the upstream region is $T_{e(0)}^{ion} = 0.025V_d$, the mode transition is entirely eliminated. This type of change thus evidently could enable stable operation over a wider range of discharge currents. A possible strategy for implementing this electron cooling could include alternative materials for the channel walls and anode (to adjust the secondary electron emission and therefore power balance in this region). Adjustments to the near-anode magnetic field similarly may impact the local electron heating.

## VII. Conclusion

In summary, in this work we have investigated parametrically the stability margin for a magnetically shielded Hall effect thruster. This was motivated by the observation that shielded thrusters appear to exhibit a transition to a high oscillatory state at high specific impulse (discharge voltage) and low power. This is a throttling condition that is desirable for deep space applications. To analyze this transition, we employed in situ plasma measurements in the thruster channel at one operating condition, $V_d = 300$ V and $I_0 = 10$ A, to motivate a simplified quasi-0D model for oscillations in discharge current and neutral density. This model has the same form as the two equation approach originally proposed by Barral [11]. In effect, this model allows for low frequency oscillations that are spontaneously excited by a feedback process between the downstream acceleration region and upstream ionization zone. This feedback is facilitated by instantaneous changes in discharge current communicated to the upstream ionization zone, which in turn leads to ionization and subsequent modulation of the neutral density flowing into the downstream acceleration region. Under the right conditions, this process can lead to positive feedback and net growth of the instability.

Armed with this result, we performed a parametric study of the discharge current oscillations in a 9-kW class Hall thruster as a function of discharge voltage and current. We then tuned our simple model by adjusting the beam utilization efficiency and neutral residence time to show that it can capture the mode transition and typical frequencies of oscillation. With this validation, we then motivated an analytical stability criteria for the mode transition and employed this to guide strategies for attempting to mitigate the mode transition. These included adjusting the magnetic field strength and modifying the anode temperature. We ultimately found that both methods can impact the discharge current where oscillations onset, lowering it by $\sim 13\%$, at a discharge voltage of $V_d = 600$ V.

We discussed the implications of our results in the context of the validity of the simplifications we made to arrive at the model as well as the implications for this result for future mitigation and ground test efforts. In particular, our result suggests possible strategies including exploring different thermal configurations and wall materials for continuing to move the transition point to lower currents. If successful, these strategies may enable the ultimate goal of a stable (defined as relative low amplitude oscillation) operation at lower power and higher specific impulse.

## Acknowledgments

This work was supported through a Strategic University Research Partnership grant from the California Institute of Technology's Jet Propulsion Laboratory. A portion of the research described here was carried out at the Jet Propulsion Laboratory, California Institute of Technology, under a contract with the National Aeronautics and Space Administration (80NM0018D0004)

## References

[1] Mikellides, I. G., Katz, I., Hofer, R. R., Goebel, D. M., De Grys, K., and Mathers, A., "Magnetic shielding of the channel walls in a Hall plasma accelerator," *Physics of Plasmas*, Vol. 18, No. 3, 2011. https://doi.org/10.1063/1.3551583.

[2] Mikellides, I. G., Katz, I., Hofer, R. R., and Goebel, D. M., "Magnetic shielding of a laboratory Hall thruster. I. Theory and validation," *Journal of Applied Physics*, Vol. 115, No. 4, 2014, pp. 0–20. https://doi.org/10.1063/1.4862313.

[3] Hofer, R. R., Goebel, D. M., Mikellides, I. G., and Katz, I., "Magnetic shielding of a laboratory Hall thruster. II. Experiments," *Journal of Applied Physics*, Vol. 115, No. 4, 2014. https://doi.org/10.1063/1.4862314.

[4] Choueiri, E. Y., "Plasma oscillations in Hall thrusters," *Physics of Plasmas*, Vol. 8, No. 4, 2001, pp. 1411–1426. https://doi.org/10.1063/1.1354644.

[5] Boeuf, J.-P., "Tutorial: Physics and Modeling of Hall Thrusters," *Journal of Applied Physics*, Vol. 121, No. 1, 2017, p. 11101. https://doi.org/10.1063/1.4972269, URL https://doi.org/10.1063/1.4972269.

[6] Fife, J., Martinez-Sanchez, M., Szabo, J., Fife, J., Martinez-Sanchez, M., and Szabo, J., "A numerical study of low-frequency discharge oscillations in Hall thrusters," *33rd Joint Propulsion Conference and Exhibit*, Joint Propulsion Conferences, American Institute of Aeronautics and Astronautics, 1997. https://doi.org/doi:10.2514/6.1997-3052, URL https://doi.org/10.2514/6.1997-3052.

[7] Boeuf, J. P., and Garrigues, L., "Low frequency oscillations in a stationary plasma thruster," *Journal of Applied Physics*, Vol. 84, No. 7, 1998, pp. 3541–3554. https://doi.org/10.1063/1.368529.

[8] Barral, S., Lapuerta, V., Sancho, A., and Ahedo, E., "Numerical Investigation of Low-Frequency Longitudinal Oscillations in Hall Thrusters," *the 29th International Electric Propulsion Conference 2005,October 31-November 4*, 2005, pp. 2005–120.

[9] Chable, S., and Rogier, F., "Numerical investigation and modeling of stationary plasma thruster low frequency oscillations," *Physics of Plasmas*, Vol. 12, No. 3, 2005, pp. 1–9. https://doi.org/10.1063/1.1857913.

[10] Barral, S., Ahedo, E., Hartfuss, H.-J., Dudeck, M., Musielok, J., and Sadowski, M. J., "On the Origin of Low Frequency Oscillations in Hall Thrusters," *AIP Conference Proceedings*, Vol. 993, 2008, pp. 439–442. https://doi.org/10.1063/1.2909170, URL http://link.aip.org/link/APCPCS/v993/i1/p439/s1&Agg=doi.

[11] Barral, S., "A new breath for the breathing mode," *31st International Electric Propulsion Conference*, , No. IEPC-2009-070, 2009.

[12] Barral, S., and Ahedo, E., "Low-frequency model of breathing oscillations in Hall discharges," *Phys. Rev. E*, Vol. 79, No. 4, 2009, p. 46401. https://doi.org/10.1103/PhysRevE.79.046401, URL https://link.aps.org/doi/10.1103/PhysRevE.79.046401.

[13] Barral, S., and Peradzyński, Z., "Ionization oscillations in Hall accelerators," *Physics of Plasmas*, Vol. 17, No. 1, 2010, p. 14505. https://doi.org/10.1063/1.3292645, URL https://doi.org/10.1063/1.3292645.

[14] Barral, S., and Miedzik, J., "Numerical investigation of closed-loop control for Hall accelerators," *Journal of Applied Physics*, Vol. 109, No. 1, 2011. https://doi.org/10.1063/1.3514151.

[15] Hara, K., Sekerak, M. J., Boyd, I. D., and Gallimore, A. D., "Mode transition of a Hall thruster discharge plasma," *Journal of Applied Physics*, Vol. 115, No. 20, 2014. https://doi.org/10.1063/1.4879896, URL http://dx.doi.org/10.1063/1.4879896.

[16] Hara, K., Sekerak, M. J., Boyd, I. D., and Gallimore, A. D., "Perturbation analysis of ionization oscillations in Hall effect thrusters," *Physics of Plasmas*, Vol. 21, No. 12, 2014. https://doi.org/10.1063/1.4903843, URL http://dx.doi.org/10.1063/1.4903843.

[17] Koshkarov, O., Smolyakov, A. I., Romadanov, I. V., Chapurin, O., Umansky, M. V., Raitses, Y., and Kaganovich, I. D., "Current flow instability and nonlinear structures in dissipative two-fluid plasmas," *Physics of Plasmas*, Vol. 25, No. 1, 2018. https://doi.org/10.1063/1.5017521, URL http://dx.doi.org/10.1063/1.5017521.

[18] Dale, E. T., and Jorns, B. A., "Two-zone Hall thruster breathing mode mechanism, Part I: Theory," *36th International Electric Propulsion Conference*, 2019, pp. 2019–354.

[19] Smolyakov, A., Romadanov, I., Chapurin, O., Raitses, Y., Hagelaar, G., and Boeuf, J. P., "Stationary profiles and axial mode oscillations in hall thrusters," *AIAA Propulsion and Energy Forum and Exposition, 2019*, , No. August, 2019, pp. 1–15. https://doi.org/10.2514/6.2019-4080.

[20] Romadanov, I. V., Smolyakov, A. I., Sorokina, E. A., Andreev, V. V., and Marusov, N. A., "Stability of Ion Flow and Role of Boundary Conditions in a Simplified Model of the E × B Plasma Accelerator with a Uniform Electron Mobility," *Plasma Physics Reports*, Vol. 46, No. 4, 2020, pp. 363–373. https://doi.org/10.1134/S1063780X20040108.

[21] Chapurin, O., Smolyakov, A. I., Hagelaar, G., and Raitses, Y., "On the mechanism of ionization oscillations in Hall thrusters," *Journal of Applied Physics*, Vol. 129, No. 23, 2021. https://doi.org/10.1063/5.0049105.

[22] Lafleur, T., Chabert, P., and Bourdon, A., "The origin of the breathing mode in Hall thrusters and its stabilization," *Journal of Applied Physics*, Vol. 130, No. 5, 2021. https://doi.org/10.1063/5.0057095.

[23] Esipchuk, Y., Morozov, A., Tilinin, G., and Trofimov, A., "Plasma oscillations in closed-drift accelerators with an extended acceleration zone," *Sov. Phys. Tech. Phys*, Vol. 18, No. 928, 1974.

[24] Darnon, F., Lyszyk, M., Bouchoule, A., Darnon, F., Lyszyk, M., and Bouchoule, A., "Optical investigation on plasma investigations of SPT thrusters," *33rd Joint Propulsion Conference and Exhibit*, 1997. https://doi.org/10.2514/6.1997-3051, URL https://arc.aiaa.org/doi/abs/10.2514/6.1997-3051.

[25] Polzin, K. a., Scooby, E. S., Raitses, Y., Merino, E., and Fisch, N. J., "Discharge Oscillations in a Permanent Magnet Cylindrical Hall-Effect Thruster," 2009, pp. 1–8.

[26] Lobbia, R. B., "A Time-resolved Investigation of the Hall Thruster Breathing Mode," *PhD Dissertation, University of Michigan*, 2010.

[27] Sekerak, M., McDonald, M., Hofer, R., and Gallimore, A., "Hall thruster plume measurements from High-speed Dual Langmuir Probes with Ion Saturation Reference," *IEEE Aerospace Conference Proceedings*, 2013. https://doi.org/10.1109/AERO.2013.6496874.

[28] McDonald, M. S., and Gallimore, A. D., "Comparison of Breathing and Spoke Mode Strength in the H6 Hall Thruster Using High Speed Imaging," *33rd International Electric Propulsion Conference*, 2013, pp. 2013–353.

[29] Sekerak, M., Longmier, B., Gallimore, A., Huang, W., Kamhawi, H., Hofer, R., Jorns, B., and Polk, J., "Mode transitions in magnetically shielded hall effect thrusters," *50th AIAA/ASME/SAE/ASEE Joint Propulsion Conference*, 2014, pp. 2014–3511. https://doi.org/10.2514/6.2014-3511.

[30] Durot, C. J., Gallimore, A. D., and Smith, T. B., "Validation and evaluation of a novel time-resolved laser-induced fluorescence technique," *Review of Scientific Instruments*, Vol. 85, No. 1, 2014. https://doi.org/10.1063/1.4856635.

[31] Lucca Fabris, A., Young, C. V., and Cappelli, M. A., "Time-resolved laser-induced fluorescence measurement of ion and neutral dynamics in a Hall thruster during ionization oscillations," *Journal of Applied Physics*, Vol. 118, No. 23, 2015. https://doi.org/10.1063/1.4937272, URL http://dx.doi.org/10.1063/1.4937272.

[32] W. Huang, Kamhawi, H., and Haag, T., "Plasma Oscillation Characterization of NASA's HERMeS Hall Thruster via High Speed Imaging," *Proceedings of the 52nd AIAA/SAE/ASEE Joint Propulsion Conference, Salt Lake City, UT*, 2016, pp. 2016–4829. https://doi.org/10.2514/6.2016-4829.

[33] Young, C. V., Fabris, A. L., Macdonald-Tenenbaum, N. A., Hargus, W. A., and Cappelli, M. A., "Time-resolved laser-induced fluorescence diagnostics for electric propulsion and their application to breathing mode dynamics," *Plasma Sources Science and Technology*, Vol. 27, No. 9, 2018. https://doi.org/10.1088/1361-6595/aade42.

[34] Raitses, Y., Romadanov, I., Smolyakov, A., Simmonds, J., and Kaganovich, I., "Hall thruster with externally driven breathing oscillations," *AIAA Propulsion and Energy Forum and Exposition, 2019*, 2019. https://doi.org/10.2514/6.2019-4078.

[35] Dale, E. T., and Jorns, B. A., "Two-zone Hall thruster breathing mode mechanism, Part II: Experiment," *36th International Electric Propulsion Conference*, 2019, pp. 1–14.

[36] Chaplin, V. H., Lobbia, R. B., Lopez Ortega, A., Mikellides, I. G., Hofer, R. R., Polk, J. E., and Friss, A. J., "Time-resolved ion velocity measurements in a high-power Hall thruster using laser-induced fluorescence with transfer function averaging," *Applied Physics Letters*, Vol. 116, No. 23, 2020, p. 234107. https://doi.org/10.1063/5.0007161.

[37] Roberts, P. J., Chaplin, V. H., Lopez Ortega, A., and Mikellides, I. G., "Impact of low-frequency oscillations on ion energy in a high-power magnetically shielded Hall thruster," *Journal of Applied Physics*, Vol. 131, No. 3, 2022. https://doi.org/10.1063/5.0067325.

[38] Dale, E. T., and Jorns, B. A., "Experimental characterization of Hall thruster breathing mode dynamics," *Journal of Applied Physics*, Vol. 130, No. 13, 2021. https://doi.org/10.1063/5.0046048.

[39] Dale, E. T., and Jorns, B. A., "Frequency scaling of the hall thruster breathing mode," *AIAA Propulsion and Energy Forum and Exposition, 2019*, , No. August, 2019, pp. 1–16. https://doi.org/10.2514/6.2019-4076.

[40] Goebel, D. M., and Katz, I., *Fundamentals of Electric Propulsion: Ion and Hall Thrusters*, 2008. URL http://www.amazon.com/Fundamentals-Electric-Propulsion-Thrusters-Technology/dp/0470429275.

[41] Dale, E. T., Jorns, B., and Hara, K., "Numerical investigation of the stability criteria for the breathing mode in Hall Effect Thrusters," *Proceedings of the 35th International Electric Propulsion Conference*, Vol. IEPC-265, 2017.

[42] Su, L. L., and Jorns, B. A., "Performance comparison of a 9-kW magnetically shielded Hall thruster operating on xenon and krypton," *Journal of Applied Physics*, Vol. 130, No. 16, 2021. https://doi.org/10.1063/5.0066849.

[43] Hofer, R., Cusson, S., Lobbia, R., and Gallimore, A., "The H9 Magnetically Shielded Hall Thruster," *Proceedings of the 35th International Electric Propulsion Conference*, 2017.

[44] Cusson, S. E., Hofer, R., Lobbia, R., Jorns, B., and Gallimore, A., "Performance of the H9 Magnetically Shielded Hall Thrusters," *Proceedings of the 35th International Electric Propulsion Conference*, 2017.

[45] Dale, E. T., and Jorns, B. A., "Non-Invasive Characterization of the Ionization Region of a Hall Effect Thruster," *54th AIAA Joint Propulsion Conference*, 2018, pp. 2018–4508. https://doi.org/10.2514/6.2018-4508, URL https://arc.aiaa.org/doi/10.2514/6.2018-4508.

[46] Cusson, S. E., Dale, E. T., Jorns, B. A., and Gallimore, A. D., "Acceleration region dynamics in a magnetically shielded Hall thruster," *Physics of Plasmas*, Vol. 26, No. 2, 2019. https://doi.org/10.1063/1.5079414.

[47] Jorns, B. A., Cusson, S. E., Brown, Z., and Dale, E., "Non-classical electron transport in the cathode plume of a Hall effect thruster," *Physics of Plasmas*, Vol. 27, No. 2, 2020. https://doi.org/10.1063/1.5130680.

[48] Su, L. L., and Jorns, B., "Performance at High Current Densities of a Magnetically-Shielded Hall Thruster," *Proceedings of the 2021 AIAA Propulsion and Energy Forum, AIAA-2021-3405*, 2021. https://doi.org/10.2514/6.2021-3405.

[49] Viges, E., Jorns, B., Gallimore, A., and Sheehan, J., "University of Michigan's Upgraded Large Vacuum Test Facility," *36th International Electric Propulsion Conference, Vienna, Austria, IEPC-2019-653*, 2019.

[50] Dankanich, J. W., Walker, M., Swiatek, M. W., and Yim, J. T., "Recommended practice for pressure measurement and calculation of effective pumping speed in electric propulsion testing," *Journal of Propulsion and Power*, Vol. 33, No. 3, 2017, pp. 668–680. https://doi.org/10.2514/1.B35478.

[51] Jorns, B. A., and Hofer, R. R., "Plasma oscillations in a 6-kW magnetically shielded Hall thruster," *Physics of Plasmas*, Vol. 21, No. 5, 2014, pp. 4–6. https://doi.org/10.1063/1.4879819.

[52] Hofer, R. R., Polk, J. E., Sekerak, M. J., Mikellides, I. G., Kamhawi, H., Sarver-Verhey, T. R., Herman, D. a., and Williams, G., "The 12.5 kW Hall Effect Rocket with Magnetic Shielding (HERMeS) for the Asteroid Redirect Robotic Mission," , No. AIAA-2016-4825, 2016. https://doi.org/10.2514/6.2016-4825, URL http://arc.aiaa.org/doi/10.2514/6.2016-4825.

[53] Book, C. F., and Walker, M. L. R., "Effect of Anode Temperature on Hall Thruster Performance," *Journal of Propulsion and Power*, Vol. 26, No. 5, 2010, pp. 1036–1044. https://doi.org/10.2514/1.48028, URL https://doi.org/10.2514/1.48028.